Dalton Transactions

An international journal of inorganic chemistry

www.rsc.org/dalton

Volume 39 | Number 26 | 14 July 2010 | Pages 5925–6128

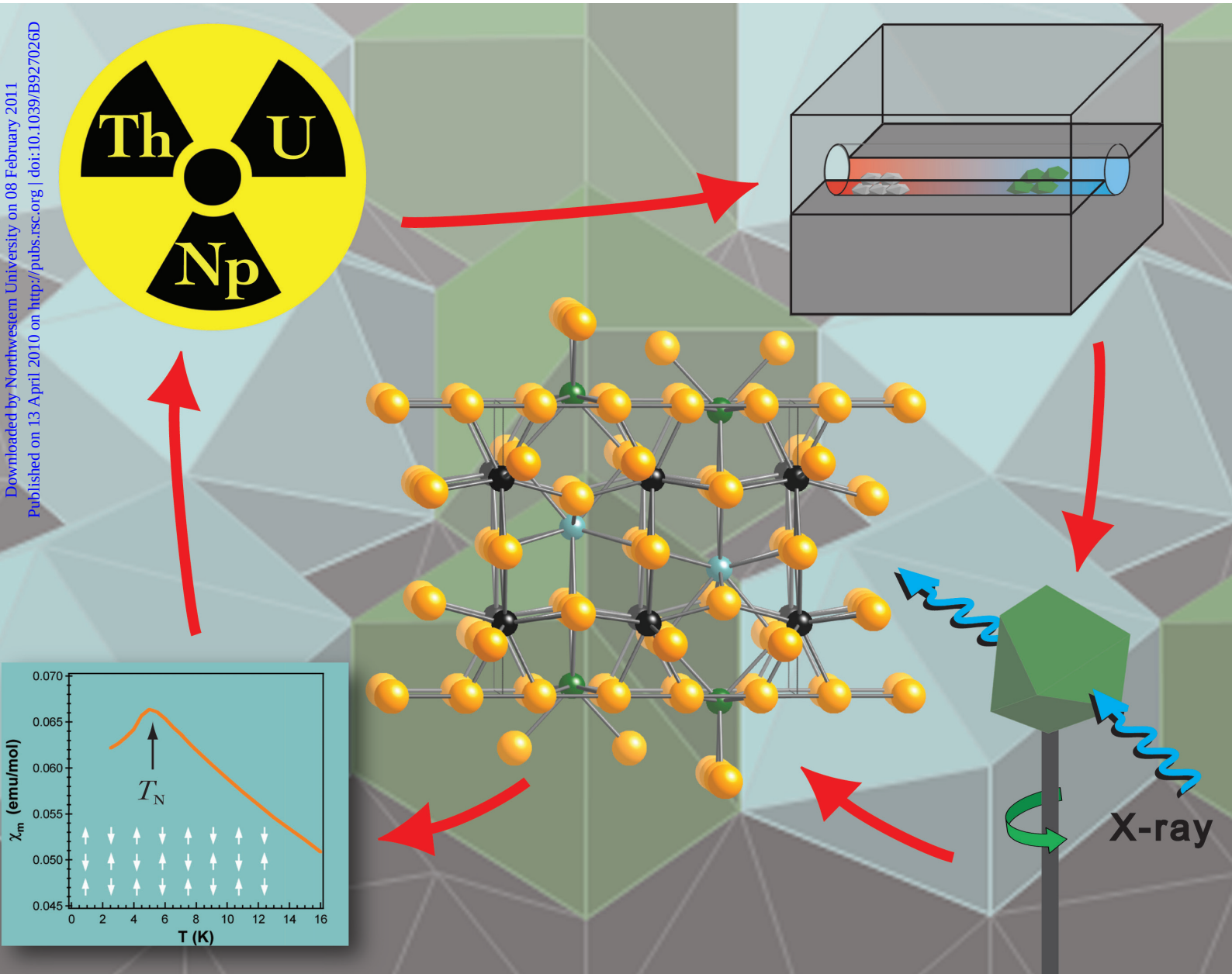

Themed issue: Frontiers of synthetic solid state chemistry

ISSN 1477-9226

RSC Publishing

This article is published as part of the *Dalton Transactions* themed issue entitled: View Online

Synthetic Solid State Chemistry

Guest Editor Duncan Gregory
University of Glasgow, UK

Published in issue 26, 2010 of *Dalton Transactions*

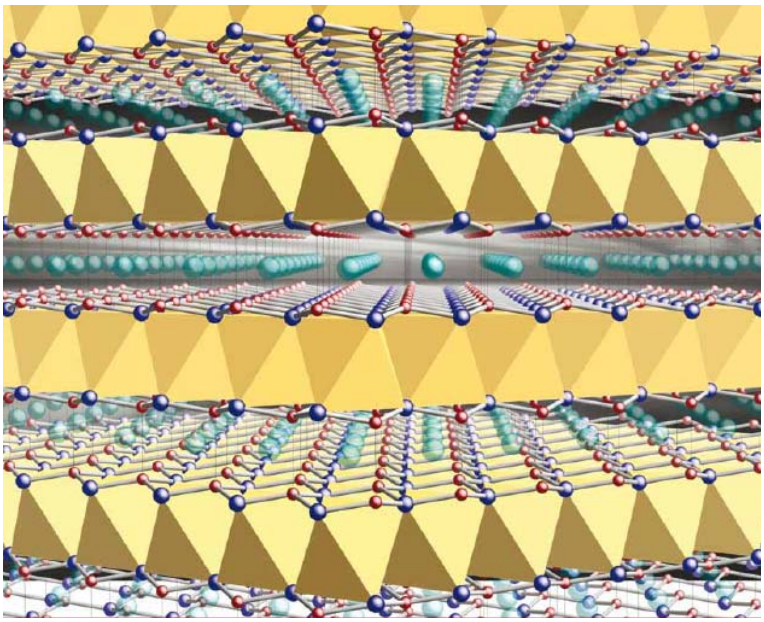

Image reproduced with the permission of Svilen Bobev

Articles in the issue include:

PERSPECTIVES:

COMMUNICATIONS:

Visit the *Dalton Transactions* website for more cutting-edge inorganic and solid-state research
www.rsc.org/dalton

Syntheses and characterization of some solid-state actinide (Th, U, Np) compounds

Daniel E. Bugaris and James A. Ibers*

Received 23rd December 2009, Accepted 4th February 2010
First published as an Advance Article on the web 13th April 2010
DOI: 10.1039/b927026d

In this Perspective we discuss a variety of methods that are broadly applicable to the syntheses of solid-state compounds. To illustrate the application of these methods we use solid-state actinide compounds, an area of chemistry that has been the focus of this laboratory for the last decade. We have synthesized single crystals, primarily of actinide chalcogenide compounds, by a variety of techniques. The benefits and drawbacks of each will be discussed in detail. Because of their propensity towards high coordination numbers and their ability to take on a variety of formal oxidation states, actinide compounds adopt structures illustrated here that are often different from those adopted by transition-metal or even lanthanide compounds. Often, there are corresponding differences in their physical properties, and these are touched upon here.

1. Introduction

As Hoffman[1] has noted, "… until you synthesize that molecule, no one can study its properties. The synthetic chemist is quite in control." The ultimate goal of solid-state chemistry is to have predictability as it pertains to the search for new materials with desired properties.[2] This goal is not yet in reach, either by theory or experiment. Thus, exploratory syntheses are essential to elucidate more fully structure–property relationships. These, in turn, provide critical calibration points for the development of effective theories of the solid-state.

We have been engaged in the syntheses and characterization of solid-state compounds for the past 25 years, with an emphasis on actinide compounds for the past 15 years. This Perspective summarizes some of our work on the actinides. For a variety of reasons, including what is in fashion and what is easier to handle, solid-state actinides have been neglected. Yet, the study of these 5f-compounds is exciting because their fundamental structures and physical properties are different from their congeners and because it is an area where experimentalists and theorists work symbiotically towards a common goal of understanding the complexities inherent in these heavy-element systems. In addition, there is, of course, the relevance of solid-state actinides to new nuclear fuel cycles in the current renaissance of nuclear energy.

Owing to their high coordination numbers and variety of accessible oxidation states (+III to +VII), the actinides often adopt intricate structure types not typically observed for the transition-metals. The physical properties of the actinides are governed by the behavior of their 5f electrons. The heavier actinides (An ≥ Am)[3] have localized 5f electrons and form An(III) ions analogous to the Ln(III) ions. The lighter actinides (Th to Pu)

Department of Chemistry, Northwestern University, Evanston, Illinois, 60208-3113, USA

Daniel E. Bugaris

Daniel E. Bugaris graduated with a B.S. in Chemistry from the University of Notre Dame (USA) in 2005, and a Ph.D. in Inorganic Chemistry from Northwestern University (USA) in 2009. His doctoral work involved the syntheses via *solid-state techniques of novel uranium halides and chalcogenides, as well as their structural characterization and measurement of physical properties. He is currently a post-doctoral fellow in the laboratory of Prof. Hans-Conrad zur Loye (University of South Carolina, USA), where his research interests are focused on the crystal growth of oxide materials for application in solid oxide fuel cells.*

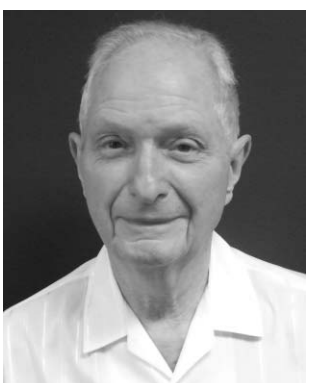

James A. Ibers

James A. Ibers received his B.S. and Ph.D. degrees from the California Institute of Technology. After a post-doctoral year at CSIRO in Melbourne, Australia, he was a chemist at Shell Development Company, then a chemist at Brookhaven National Laboratory, before moving to Northwestern University where he is currently the Charles E. and Emma H. Morrison Professor of Chemistry. His current research interests are the topic of this Perspective. He is a member of the American Academy of Arts and Sciences and of the U.S. National Academy of Sciences.

have 5f electrons whose behavior tends to be intermediate between the itinerant d electrons of the transition-metals and the more localized 4f electrons of the lanthanide elements. This itinerancy can give rise to interesting properties in the early actinides, such as heavy fermion behavior in UBe_{13}[4] and UPt_3,[5] superconductivity in $NpMo_6Se_8$[6,7] and $PuCoGa_5$,[8] and most recently heavy fermion superconductivity in $NpPd_5Al_2$.[9] Th and U compounds can be handled within normal laboratory facilities; Np, and especially Pu, compounds require more specialized facilities. All four elements are much more readily available than the heavier actinides. Thus, these earlier actinides are of particular interest.

Our investigation of the actinides has focused on the chalcogenides and pnictides, as well as on oxychalcogenides and oxypnictides, neglected areas compared to actinide-containing oxides and intermetallics. Whereas a search of the Inorganic Crystal Structure Database reveals numerous actinide oxides and intermetallics, comparatively few chalcogenide and pnictide compounds are found, particularly in ternary and higher multinary systems. In addition to gaining a better understanding of the chemistry among actinides, chalcogenides, and pnictides, there are additional reasons for our interest in them. First, unlike oxygen, which is found only as discrete O^{2-} anions (except in solid-state peroxides), the chalcogens and pnictogens can also form dianions (*i.e.*, S_2^{2-}) as well as higher order polyanions (chains or nets). These unusual bonding modes can combine with the high coordination environments of the actinides to yield highly complex structures. Second, the softer chalcogenide and pnictide anions, as opposed to the hard oxide anion, can produce a greater variety of oxidation states in the actinides. For example, nearly all uranium oxide compounds contain the linear uranyl (UO_2^{2+}) cation and hence U(VI). Such f^0 compounds are relatively uninteresting magnetically (diamagnetic) and electrically. However, with chalcogenide ligands, U is known to adopt oxidation states of +III, +IV, and +V, and display a variety of exciting magnetic and transport properties.

Now for some caveats. With respect to syntheses, a caveat enunciated by DiSalvo[10] two decades ago summarized the well-known problems and the excitement of solid-state synthesis: "Yet many basic principles and concepts that serve well other branches of chemistry…are lacking or only apply to a small fraction of solid-state compounds. These include the ability to understand and predict composition,… structure,… and reaction pathways… In general, our predictive ability is almost non-existent… this lack of understanding is a source of not only great challenge, but also of surprise, wonder, and excitement about the intricacy of nature. Thus, the science of solid-state chemistry includes elements of "art," such as intuition and insight based on experience rather than the use of predictive models." In the intervening 20 years some progress has been made, but DiSalvo's remarks remain germane. The impact of kinetics or thermodynamics on a particular reaction cannot be noted with certainty, and therefore the reaction method may be chosen somewhat arbitrarily, or several reaction methods may be employed until one proves successful. Sorting through the diverse variables is where the "art" comes in. These variables in a solid-state reaction that is to be carried out in a high temperature furnace include but are not limited to: starting reagents and their purities, stoichiometric ratios of starting reagents, masses of starting reagents, how well the starting reagents are mixed prior to the reaction, type of vessel for the reaction, size of vessel for the reaction, orientation of the vessel for the reaction (horizontal, vertical, or somewhere in between), rate of heating, maximum reaction temperature, length of time at maximum reaction temperature, and cooling rate. Perhaps our favorite (or is it our least favorite?) variable is the identity of the furnace in which the reaction takes place. On occasion, a reaction will only yield the desired product when performed in a certain "magic" furnace. We presume that the heating element(s) in this furnace have aged differently from those in another furnace, or the electronic display of the temperature is slightly off, such that a given temperature in this "magic" furnace is not equivalent to the same temperature in another furnace. If the reaction is to be carried out in an arc melter or by solvothermal means, techniques that are not discussed in this Perspective, then some of these variables apply as well and new ones arise.

A caveat with respect to structure determinations: powder samples are easier to prepare than single crystals. (It is debatable whether the preparation of "phase pure" powders is easier or not.) However, single crystals are generally pure, whereas powders often contain variable amounts of extra phases. Consequently, as a matter of course we have used only single crystals in our structure determinations. Our X-ray data collections are typically performed at low temperatures (100 K or 153 K), which reduces thermal motion of the atoms and provides for better structure refinements. One of the drawbacks of collecting X-ray diffraction data at low temperatures is that we may not observe possible higher temperature structural transitions.

A caveat with respect to the measurement of physical properties: the requirement that we measure physical properties on single crystal samples is sometimes severely limiting. Although optical measurements can be made on one single crystal (even the same one used for the collection of X-ray diffraction data), electrical conductivity and magnetic susceptibility measurements have more stringent demands. Electrical conductivity can be measured on one single crystal, but the crystal must be large enough to accommodate four conducting leads. This necessitates a crystal of at least 0.3 mm in length and an experienced (and steady) hand, but more often ~1 mm is an appropriate size. We have found that magnetic susceptibility requires, at the bare minimum, 5 mg of sample for reliable, reproducible results. Although this seems like a simple requirement to meet, it is often rather difficult. Because of the limited availability of the actinide metals, our reactions start with no more than 30 mg of Th or U and 20 mg of Np. Furthermore, a reaction with a 25% yield is considered a success, and of that 25% yield, not all of the product can be manually separated with certainty from the byproducts or flux. Because of our limited supply of starting materials, we cannot afford to run multiple experiments in order to maximize yields.

With those caveats in mind, we proceed. In this Perspective, we will discuss the solid-state syntheses of a number of actinide compounds (Table 1) by the following methods: combination of the elements (2.1), chemical vapor transport (2.2), alkali-metal polychalcogenide reactive fluxes (2.3), alkali-metal or alkaline-earth-metal halide salt fluxes (2.4), antimony chalcogenide fluxes (2.5), tin fluxes (2.6), and metathesis reactions (2.7). Serendipitous results are examined in 2.8. The structures, and where applicable, the physical and theoretical properties of these compounds will also be discussed. Within these sections, the results will be discussed chronologically. However, the compounds in Table 1 have

Table 1 Actinide compounds discussed in this Perspective

Compound/s	Synthesis[a]	Structure	An geometry[b]	An oxidation state	Properties[c]	Section/s	Figure
AAn_2Q_6	ampc, h, s	layered	btp	+IV	ec, ms, opt	2.3.5, 2.4.7, 2.8.2, 2.8.7	12
$AMAnQ_3$	ampc, h	layered	oct	+IV	ec, ms, t	2.3.4, 2.4.4, 2.4.5	11
$Ba_4Cr_2US_9$	s	chains	tp	+IV	—	2.8.5	25
$Ba_2Cu_2US_5$	h	layered	oct	+IV	ms	2.4.3	15
$Ba_8Hg_3U_3S_{18}$	h	chains	oct	?	ms	2.4.6	16
CuAnOP	cvt	layered	sa	+IV	ec, ms, nd, t	2.2.4, 2.2.5	7
$Cu_xAn_2Te_6$	e, h	layered	btp	?	ec, ms	2.1.1, 2.4.2	1
$CuNpSe_2$	cvt	layered	mtp	+III	—	2.2.3	6
$Cu_{0.60}USb_2$	s	layered	sa	+IV	—	2.8.4	24
$Cs_8Hf_5UTe_{30.6}$	ampc	chains	tp	?	—	2.3.3	10
$Cs_2Hg_2USe_5$	ampc	layered	oct	+IV	ec, ms	2.3.6	13
$CsMUTe_5$	ampc	layered	btp	?	ec, ms	2.3.2	9
$CsUTe_6$	ampc	chains	ttp	+IV	ec	2.3.1	8
$[Hg_4As_2][UCl_6]$	cvt	3D	oct	+IV	opt	2.2.2	5
$[Hg_3Te_2][UCl_6]$	cvt	layered	oct	+IV	ms, opt	2.2.1	4
$K_2Cu_3US_5$	m	layered	oct	+V	esr, ms	2.7.1	21
$La_2U_2Se_9$	ac	3D	msa	+IV	ms, s, sh	2.5.3	19
$Ln_2UO_2S_3$	ac	layered	sa	+IV	ms, opt	2.5.2	18
MUQ_3	e, h, t	3D	btp	+IV	—	2.1.2, 2.4.1, 2.6.2	2
$Rb_6Cu_{12}U_2S_{15}$	ampc	3D	oct	+V or +VI	ms	2.3.7	14
$SrTh_2Se_5$	t	3D	btp, mtp	+IV	—	2.6.1	20
$[Ta_7(Se_2)_{14}][U_2I_{10}]_2$	e	chains	oct	+IV	—	2.1.3	3
$Ta_2UO(S_2)_3Cl_6$	s	chains	complex	+IV	opt, t	2.8.6	26
UOSe	s	3D	ttp	+IV	—	2.8.1	22
US_3	s	layered	btp	+IV	—	2.8.3	23
$Y_4UO_3S_5$	ac	3D	ctp, sa	+IV	ec, ms	2.5.1	17

[a] Synthesis – ac: antimony chalcogenide; ampc: alkali-metal polychalcogenide; cvt: chemical vapor transport; e: elements; h: alkali-metal or alkaline-earth-metal halide; m: metathesis; s: serendipity; t: tin. [b] Actinide geometry – btp: bicapped trigonal prism; fco: face-capped octahedron; msa: monocapped square antiprism; mtp: monocapped trigonal prism; oct: octahedron; sa: square antiprism; ttp: tricapped trigonal prism. [c] Properties – ec: electrical conductivity; esr: electron spin resonance; ms: magnetic susceptibility; nd: neutron diffraction; opt: optical band gap; s: spectroscopy (*e.g.* XANES); sh: specific heat; t: theoretical calculations

been listed alphabetically, as a convenience for those interested in particular compounds.

In the drawings of the structures the following convention has been utilized to identify the elements: actinide = black; alkali-metal = blue; alkaline-earth-metal = light blue; chalcogen = orange; halide = purple; lanthanide = gray; oxygen = red; pnictogen = pink; transition-metal = green.

2. Solid-state syntheses, structures, and characterization

^{232}Th and ^{238}U are α-emitting radioisotopes, and ^{237}Np is an α- and γ-emitting radioisotope; as such, they are considered health risks. Their use requires appropriate infrastructure and personnel trained in the handling of radioactive materials. For our work with Th and U compounds reaction vessels are typically standard carbon-coated fused-silica ampules. Standard computer-controlled high temperature furnaces are employed. For our work with Np compounds, in order to minimize the risk of reaction-vessel failure, all reaction vessels consist of primary and secondary containment. Primary containment is supplied by standard carbon-coated fused-silica ampules. Secondary containment comprises a combination of mechanical containment that consists of stainless steel tubing with tongue and groove caps and chemical containment that is provided by a second larger fused-silica ampule. Further precautions are taken by heating all reactions in a computer-controlled high temperature furnace equipped with both standard and runaway controllers. The furnace is inside a negative-pressure hood.

Although certain actinide compounds are available commercially (ThO_2, UO_3, $UO_2(CH_3COO)_2{\cdot}2H_2O$, $UO_2(NO_3)_2$), actinide metals must be obtained through other avenues. Much of the ^{232}Th work was done pre-9/11 when it could still be purchased from commercial suppliers. The metallic ^{238}U and ^{237}Np were procured from Oak Ridge National Laboratory in the form of depleted turnings and brittle chunks, respectively. The U turnings were found by experiment to be relatively unreactive, having low surface area and being coated with a layer of oxide. This situation was remedied by using a modified literature procedure[11] to produce U powder. The U turnings were washed with concentrated HNO_3 acid to remove the oxide coating, rinsed with de-ionized water, and dried with acetone. The turnings were then placed in a Schlenk tube, and exposed to a H_2 atmosphere at 723 K to produce UH_3. The UH_3 was decomposed under vacuum to give pure U powder.

Other U starting materials can also be prepared. UCl_4 may be synthesized by refluxing UO_3 with hexachloropropene at 431 K.[12] Binary U chalcogenides and pnictides may be prepared by the stoichiometric reactions of the elements in sealed tubes at appropriate temperatures.[13] UOS may be synthesized by reacting UO_2 with S in a carbon crucible within a sealed tube at 1213 K.[14]

2.1 Compounds synthesized from the elements

Traditionally, solid-state chemistry has involved the high temperature fusion of elements or binary compounds (*i.e.*, metal oxides, sulfides, phosphides) to produce higher-order compounds.

Very high temperatures, typically in excess of 1273 K, as well as long reaction times (weeks or months) are necessary to overcome the thermodynamic and kinetic barriers to product formation. These barriers can include high melting points of the reactants, low diffusion coefficients, and the tendency for reactions to attain equilibrium with only binary phase formation. All of these obstacles contribute to the somewhat arbitrary results of high temperature syntheses ("shake 'n bake").

In high temperature syntheses the reactions can be performed in closed or open vessels depending upon the stability of the reactants and products on exposure to air. Examples of containers for closed systems include sealed tubes made of fused silica or refractory metals (such as Ta); open vessels are primarily alumina or precious-metal crucibles. The choice of appropriate containment for the reaction is dictated by both the stability of the vessel and the reactivity of the reagents. For example, fused silica begins to soften at about 1500 K, necessitating the use of metal tubes for reactions at higher temperatures. Furthermore, if the starting reagents are sufficiently reactive, they may absorb oxygen from fused silica or alumina; this can be avoided by the use of refractory or precious-metal vessels.

The syntheses by combination of elements or binary compounds usually leads to powders rather than single crystals. Without the addition of a vapor transport or fluxing agent, the majority of combination reactions yield powder samples. To form a single crystal of the desired product, at least one of the components of the reaction should be molten at the maximum reaction temperature. Otherwise, a single crystal can be grown from a powder by high temperature annealing for a significant length of time.

2.1.1 $CuTh_2Te_6$[15]. Single crystals of $CuTh_2Te_6$ formed in high yield by a stoichiometric reaction of the elements at 1273 K. The compound crystallizes in space group $P2_1/m$ in a new structure type. The structure (Fig. 1) consists of layers of $^2_\infty[Th_2Te_6^-]$ double chains joined by Cu^+ cations. Each Th atom is coordinated to eight Te atoms in a bicapped trigonal-prismatic arrangement. There are three crystallographically unique Te atoms. Each $ThTe_8$ unit is bridged through one distinct Te atom, such that the capping Te atom of one unit forms the vertex of its neighbor. The two non-bridging Te atoms form infinite Te–Te chains along the exterior of the $^2_\infty[Th_2Te_6^-]$ layer. Copper atoms are coordinated to these Te atoms in a tetrahedral arrangement. Owing to the existence of Te–Te bonds of intermediate length, the assignment of formal oxidation states in this compound is not possible. Two-probe dc resistivity measurements on a single crystal of $CuTh_2Te_6$ showed it to be a semiconductor along [010]. Magnetic susceptibility measurements in the range 2–300 K showed $CuTh_2Te_6$ to be paramagnetic.

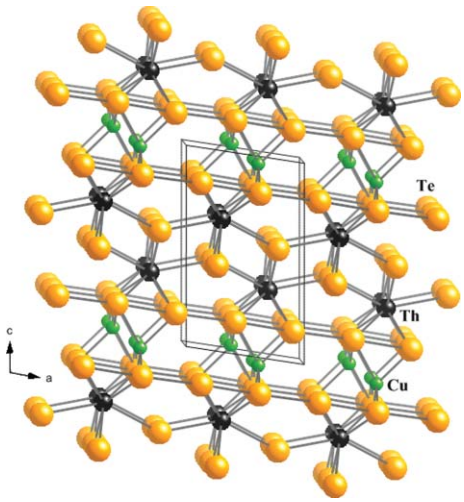

Fig. 1 Unit cell of $CuTh_2Te_6$ as viewed along [010]. Here, and in successive figures, actinide = black; alkali-metal = blue; alkaline-earth-metal = light blue; chalcogen = orange; halide = purple; lanthanide = gray; oxygen = red; pnictogen = pink; transition-metal = green.

2.1.2 $MnThTe_3$[16]. The compound was synthesized as small black needles in very high yield from the stoichiometric reaction of the elements at 1273 K. $MnThTe_3$ crystallizes in space group *Cmcm* in the $FeUS_3$ structure type,[17] as do $MnThSe_3$ (2.6.2), $MgThTe_3$ (2.6.2), and $MnUSe_3$ (2.4.1). The structure (Fig. 2) is pseudo-layered with slabs of corner-shared $MnTe_6$ octahedra alternating with slabs of cap- and edge-shared $ThTe_8$ bicapped trigonal prisms. The slabs are bonded together through the sharing of edges and vertices of the various polyhedra to form a three-dimensional structure.

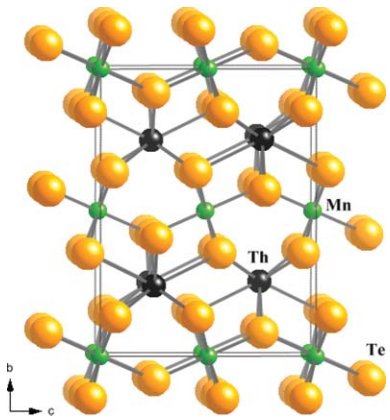

Fig. 2 Unit cell of $MnThTe_3$ as viewed down [100].

2.1.3 $[Ta_7(Se_2)_{14}][U_2I_{10}]_2$[18]. In an investigation of the U/Ta/Se system a reaction was carried out among U, Ta, and Se at 1173 K with I_2 added as a transport agent. The resultant compound, $[Ta_7(Se_2)_{14}][U_2I_{10}]_2$, because it was obtained serendipitously in low yield by vapor transport, could equally well have been placed in 2.2 or 2.8. It crystallizes in space group *Cccm* in a new structure type. The crystal structure (Fig. 3) comprises infinite $[Ta(Se_2)_2]_n$ cationic chains charge balanced by $[U_2I_{10}]^{2-}$ anions. The previously unknown $[U_2I_{10}]^{2-}$ anion is formed by two edge-sharing UI_6 octahedra. The U–I bond distances are normal for tetravalent U. It is not often that one has the pleasure of synthesizing a previously unknown binary anion! For charge balance, the $[Ta_7(Se_2)_{14}]^{4+}$ cation must contain three Ta(IV) and four Ta(V) centers. Charge is delocalized over this cation as the Ta · · · Ta interactions differ minimally.

2.2 Compounds synthesized by chemical vapor transport

Chemical vapor transport reactions[19] use a reagent in the vapor phase to transport a material from a reaction zone through a temperature gradient to another zone, where it deposits in

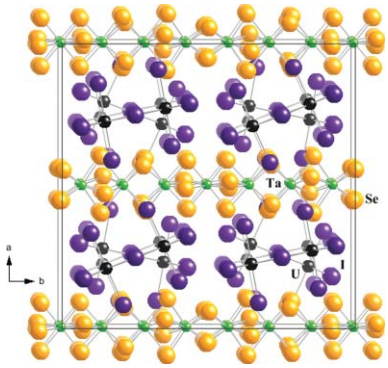

Fig. 3 Unit cell of $[Ta_7(Se_2)_{14}][U_2I_{10}]_2$ as viewed along [001].

crystalline form. The temperature gradient, which can range from 50 to 200 K, reflects the thermodynamic stability of the reactants and products. For endothermic reactions, the product crystallizes in the cooler zone, whereas for exothermic reactions the product crystallizes in the warmer zone.

Once again, the reactions can be performed in "open" or closed systems. The "open" system is typically a tube furnace with a temperature gradient through which a carrier gas can be flowed. Examples of gases used for these chemical vapor transport reactions include O_2, Cl_2, HCl, NH_3, or H_2O. In a closed system a sealed fused-silica tube is placed in a furnace such that one end of the tube is located in the warmer zone and the opposite end in the cooler zone. Vapor transport agents utilized in sealed systems are most often solids that volatilize upon heating, such as I_2, $TeCl_4$, or d- or f-block metal-halides.

The disadvantage of chemical vapor transport is that it is more of a crystallization technique than a synthetic method. There are instances of the synthesis of new materials with the use of chemical vapor transport. Typically, however, chemical vapor transport requires a phase-pure powder (from a combination reaction) that can then be crystallized by its reaction with a volatile transport agent. Even if the powder is not phase-pure, in some instances a purification process takes place so that crystals of the desired product are obtained and impurities are left behind. In a sense, this is akin to the purification of molecular materials by re-crystallizing them from selected solvents.

2.2.1 $[Hg_3Te_2][UCl_6]$[20]. Green single crystals of $[Hg_3Te_2][UCl_6]$ were obtained in about 70% yield from the stoichiometric reaction of UCl_4, $HgCl_2$, and HgTe at 873 K, with volatile $HgCl_2$ (bp = 575 K) acting as the transport agent. The compound crystallizes in space group $P2_1/c$. The structure (Fig. 4) comprises a two-dimensional framework of $^2_\infty[Hg_3Te_2^{2+}]$ layers with discrete $[UCl_6]^{2-}$ anions between the layers. $[Hg_3Te_2][UCl_6]$ exhibits temperature-independent paramagnetism, as obtained from measurements on ground single crystals. The optical absorption spectrum of a single crystal displays f–f transitions and a band gap of about 2.6 eV.

2.2.2 $[Hg_4As_2][UCl_6]$[20]. Red block-shaped crystals of $[Hg_4As_2][UCl_6]$ were obtained in about 80% yield from the reaction of U, Hg_2Cl_2, and As at 788 K. In this reaction, Hg_2Cl_2, which sublimes at 673 K, serves as the transport agent. The compound crystallizes in space group *Pbca*. The structure of $[Hg_4As_2][UCl_6]$ (Fig. 5) has a three-dimensional framework of $^2_\infty[Hg_3As_2]$ layers interconnected by Hg atoms linearly bonded to

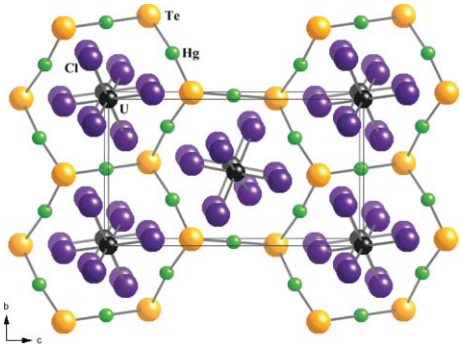

Fig. 4 Unit cell of $[Hg_3Te_2][UCl_6]$ as viewed along a^*.

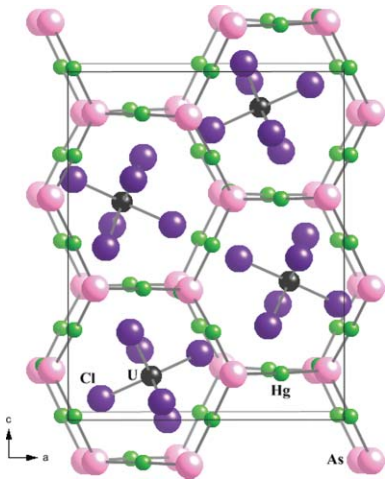

Fig. 5 Unit cell of $[Hg_4As_2][UCl_6]$ as viewed down [010].

As atoms. The optical absorption spectrum of a single crystal displays f–f transitions and a band gap of approximately 1.9 eV.

2.2.3 $CuNpSe_2$[21]. $CuNpSe_2$ was formed in an attempted synthesis of the Np analogue of $Cu_2U_3Se_7$.[22] $CuNpSe_2$ is the first ternary neptunium transition-metal chalcogenide to be synthesized. This was done by the reaction of Np, Cu, and Se at 873 K. Single crystals were grown by vapor transport with I_2. The compound crystallizes in the $CuLaS_2$ structure type (Fig. 6)[23] in space group $P2_1/c$. It can be viewed as a stacking along [100] of layers of $CuSe_4$ tetrahedra and of double layers of $NpSe_7$ monocapped trigonal prisms. Because there are no Se–Se bonds in the structure, the formal oxidation states of Cu/Np/Se may

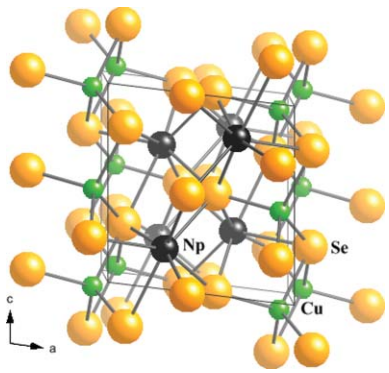

Fig. 6 Unit cell of $CuNpSe_2$ as viewed down [010].

be assigned as +I/+III/−II, respectively. We note in passing that Cu is invariably in the +I oxidation state in copper-containing chalcogenides.

2.2.4 CuUOP[24]. The original synthesis[25] of CuUOP involved the reaction of UP and CuO, followed by vapor transport with I_2 to afford single crystals. Attempted synthesis of CuUOP using this method was unsuccessful. We found that the reaction of U, CuO, Cu, and P at 1273 K afforded a black powder that contained mainly CuUOP. This product was loaded into a fused-silica ampule with I_2. It was heated in a two-zone furnace at 1173/1223 K to afford thin black rectangular plates of CuUOP in moderate yield, but because most of the single crystals synthesized were too small to be extracted cleanly from the product mixture the extracted yield was less than 5%. Failure to prepare a material from a literature procedure is not unusual. Differences in any number of variables, including purities of the starting materials, furnaces, and techniques, can be responsible.

CuUOP crystallizes in space group *P*4/*nmm* with the CuZrSiAs structure type (Fig. 7).[26] Each U atom is coordinated to four O and four P atoms in a distorted square antiprism; each Cu atom is coordinated to four P atoms in a distorted tetrahedron. Magnetic susceptibility measurements on crushed single crystals indicated that CuUOP orders antiferromagnetically at 224(2) K. Neutron diffraction experiments on CuUOP powder at 100 K and 228 K showed the magnetic structure of CuUOP to be type-AFI (+ − + −) where ferromagnetically aligned sheets of U atoms in the (001) plane order antiferromagnetically along [001]. From measurements on single crystals the electrical resistivity of CuUOP increases with temperature in the antiferromagnetically ordered region then becomes nearly temperature independent in the paramagnetic region. The trend is similar to that of UP_2.[27,28]

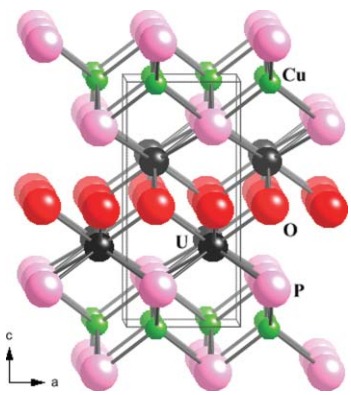

Fig. 7 Unit cell of CuUOP as viewed along [010].

2.2.5 CuNpOP[24]. A reaction mixture of Np, CuO, and P was heated to 1073 K to afford a black powder. This powder and I_2 were heated together to 823 K to afford thin black rectangular plates of CuNpOP in moderate yield but, as with CuUOP, most of the crystals were very small which made a clean separation from the product mixture difficult. The estimated yield of separated mass was less than 5%. The crystals used in characterization were manually extracted from the product mixture. CuNpOP is isostructural with CuUOP (2.2.4 and Fig. 7). Calculations on a 2 × 2 × 2 supercell of CuNpOP within the LSDA + GGA framework show ferromagnetic ordering within the Np sheets and complex ferromagnetism between.

Table 2 Melting points (K) of some alkali-metal polychalcogenides (A_2Q_x)

		Na	K	Rb	Cs
A_2Q	S	1453[a]	1113[a]	803[a]	
	Se	1148[a]	1073[c]	793[c]	1043[b]
	Te	1226[a]			1093[d]
A_2Q_3	S	501.8[a]	525[a]	486[a]	490[a]
	Se	586[a]	653[a]		611[b]
	Te			538[c]	668[d]
A_2Q_5	S	524.8[a]	479[a]	498[a]	483[a]
	Se		463[a]		515[b]
	Te				508[d]

[a] Ref. 80. [b] Ref. 81. [c] Ref. 82. [d] Ref. 83.

2.3 Compounds produced with alkali-metal polychalcogenide reactive fluxes

Alkali-metal polychalcogenides of the general formula A_2Q_x (A = Li, Na, K, Rb, Cs; Q = S, Se, Te) have been used as reactive fluxes[29,30] for the syntheses and crystallization of novel ternary and quaternary chalcogenide materials. The attraction of using alkali-metal polychalcogenide reactive fluxes is that their melting points range from approximately 400 to 1400 K (Table 2). This versatility allows reactions to be performed at low and intermediate temperatures where interesting kinetic products can be isolated, as well as high temperatures where the most thermodynamically stable compounds can be obtained.

The A_2Q_x compounds (other than Li_2S and Na_2S) are not available commercially and must be synthesized. This is done most conveniently from the stoichiometric addition of the elements in liquid NH_3 at 194 K. Because the alkali-metal polychalcogenides are extremely air- and moisture-sensitive, all reactions with them must be performed under inert conditions, typically in sealed fused-silica tubes. Also, the A_2Q_x compounds are highly reactive, so fused-silica tubes, if used, must be carbon-coated. Failure to do this may result in the incorporation of silicon or oxygen or both into the products, or explosion of the tubes. Upon completion of the reaction, the desired crystalline product can be isolated by dissolving the excess alkali-metal polychalcogenide flux in a polar solvent, such as *N*,*N*-dimethylformamide.

2.3.1 $CsUTe_6$[31]. The compound $CsUTe_6$ was obtained in low yield from the reaction of Ag, U, Te, and Cs_2Te_3 at 1173 K. The target quaternary compound of Cs, U, Ag, and Te did not form; other products included binaries and the ternary compound $CsAg_5Te_3$. $CsUTe_6$ crystallizes in space group *Pnma*. It has a one-dimensional structure (Fig. 8) that contains pairs of U/Te chains coupled by Te–Te bonds and separated by Cs^+ cations. There are many Te–Te distances less than 3.1 Å; if an arbitrary maximum Te–Te single bond distance is taken as 2.98 Å, then the chains may be formulated $^1_\infty[U_2(Te_3)_3(Te_2)(Te)^{2-}]$, with U in the +IV oxidation state. The U atoms are coordinated to nine Te atoms in a tricapped trigonal-prismatic arrangement. Electrical resistivity measurements gave conductivities of $1.6(4) \times 10^{-2}$ S cm^{-1} (298 K) and $1.5(2) \times 10^{-3}$ S cm^{-1} (77 K).

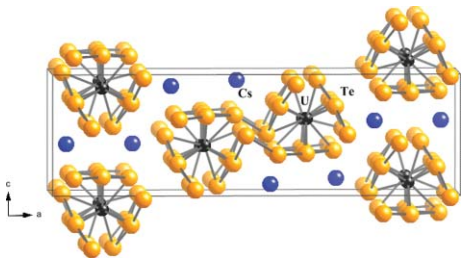

Fig. 8 Unit cell of $CsUTe_6$ as viewed down [010].

2.3.2 $CsTiUTe_5$[31] and $CsZrUTe_5$[32]. The compound $CsTiUTe_5$ was synthesized through the stoichiometric reaction at 1173 K of the metals with a Cs_2Te_3 flux. $CsTiUTe_5$ crystallizes in space group *Pmma*. $CsTiUTe_5$ has a layered structure (Fig. 9) that contains UTe_8 bicapped trigonal prisms sharing a common edge and $TiTe_6$ octahedra sharing faces. Cs^+ cations, located in pentagonal prisms of Te atoms, separate the layers. The structure contains an infinite linear Te–Te chain in which the Te atoms are separated by 3.065(1) Å. Assignment of formal oxidation states from the structural results is difficult owing to the presence of Te–Te bonding. $CsZrUTe_5$ was synthesized at 1223 K from the reaction of Cs_2Te_3, U, Zr, and excess CsCl. It is isostructural with $CsTiUTe_5$.

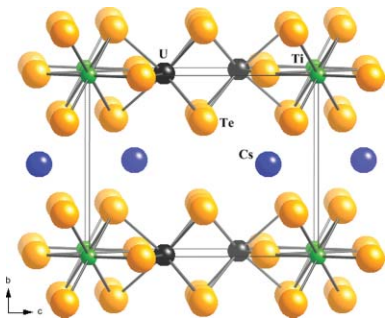

Fig. 9 Unit cell of $CsTiUTe_5$ as viewed along [100].

Magnetic susceptibility data for $CsTiUTe_5$ gave a curvilinear χ^{-1} *versus* T plot. When fit to a modified Curie–Weiss law, the values $C = 8.8(3) \times 10^{-2}$ emu K mol^{-1}, $\theta = -1.5(2)$ K, and $\chi_0 = 2.11(8) \times 10^{-3}$ emu mol^{-1} resulted. The value of μ_{eff} (300 K) is 2.23(1) μ_B for each $CsTiUTe_5$ unit. The resistivity of $CsTiUTe_5$ at 77 K was beyond the detection limits of the instrument, but it was $1.2(9) \times 10^{-3}$ S cm^{-1} at 298 K.

2.3.3 $Cs_8Hf_5UTe_{30.6}$[31]. In an attempt to synthesize the Hf analogue of the two-dimensional compound $CsTiUTe_5$, the compound $Cs_8Hf_5UTe_{30.6}$ was synthesized. It was prepared in low yield from the reaction of the elements and Cs_2Te_3 at 973 K. $Cs_8Hf_5UTe_{30.6}$ crystallizes in space group $P2_1/c$. It forms a one-dimensional structure (Fig. 10) with ordered Hf and U atoms and disordered Te atoms in two unique chains that may be formulated as $^1_\infty[Hf_3Te_{15.6}^{4-}]$ and $^1_\infty[Hf_2UTe_{15}^{4-}]$. Cs^+ cations separate the chains. The Hf and U atoms are coordinated to Te atoms in a distorted trigonal-prismatic framework. Because there are many short Te–Te distances, the assignment of formal oxidation states is not possible.

2.3.4 $AMAnQ_3$[16,31,33-36]. The compounds $AMAnQ_3$ were synthesized by the reaction of the metals with an A_2Q_x flux at temperatures ranging from 793 to 1173 K. The Th[16] and Np[36] compounds synthesized by us include $KCuThSe_3$, $CsCuThSe_3$, $KCuNpS_3$, $RbCuNpS_3$, $CsCuNpS_3$, $KAgNpS_3$, and $CsAgNpS_3$, whereas the known U compounds are summarized in Table 3. These compounds crystallize in space group *Cmcm* in the $KCuZrS_3$ structure type,[37] with A atoms substituted for K atoms and An atoms substituted for Zr atoms. This structure type is adopted by a multitude of $AMM'Q_3$ compounds, where A is an alkali-metal or alkaline-earth-metal, M is a transition-metal, M′ is a lanthanide or an actinide, and where the formal oxidation states of A, M, and M′ sum to +VI. The structure comprises $^2_\infty[MAnQ_3^-]$ layers alternating with A^+ cations stacked in the [010] direction (Fig. 11). These layers are formed by alternating ribbons of AnQ_6 octahedra and MQ_4 tetrahedra. The AnQ_6 octahedra edge-share in the [100] direction and corner-share in the [001] direction with other AnQ_6 octahedra. The M atoms sit in tetrahedral holes, edge-sharing with four AnQ_6 octahedra in the (010) plane and corner-sharing with two M tetrahedra in the [100] direction. Each A atom is coordinated in a bicapped trigonal-prismatic environment by eight

Table 3 Known compounds in the $AMUQ_3$ family

	Cu	Ag	Au
K	S[a], Se[b]		
Rb	S[a]	S[a], Se[a]	Se[c], Te[c]
Cs	S[a], Se[d], Te[e]	S[a], Se[a]	Se[c], Te[c]

[a] Ref. 34. [b] Ref. 84. [c] Ref. 35. [d] Ref. 33. [e] Ref. 31.

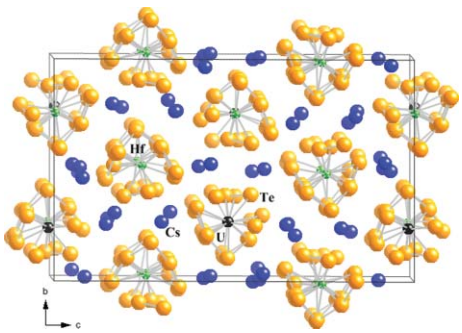

Fig. 10 Unit cell of $Cs_8Hf_5UTe_{30.6}$ as viewed down a^*.

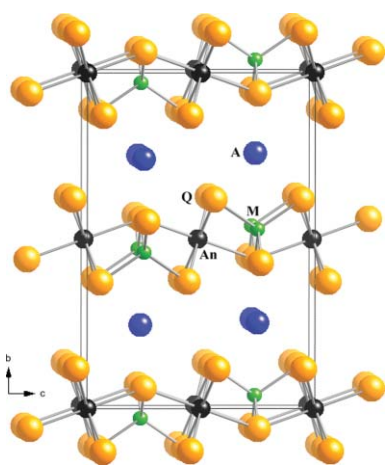

Fig. 11 Unit cell of $AMAnQ_3$ (A = K, Rb, Cs; M = Cu, Ag, Au; An = Th, U, Np) as viewed along [100].

Q atoms. Because there are no Q–Q bonds, the formal oxidation states of A/M/An/Q may be assigned as +I/+I/+IV/–II.

Only a limited number of physical measurements or theoretical calculations have been performed on these compounds. $CsCuUS_3$[34] shows semiconducting behavior with thermal activation energy E_a = 0.14 eV and σ_{298} = 0.3 S cm^{-1}. From single-crystal absorption measurements in the near IR range the optical band gaps of the $AMUS_3$ (A = Rb, Cs; M = Cu, Ag) compounds are smaller than 0.73 eV.[34] The more diffuse 5f electrons play a much more dominant role in the optical properties of the $AMUQ_3$ compounds than do the 4f electrons in the $AMLnQ_3$ compounds. Density-of-states analysis[34] for $CsCuUS_3$ and $CsAgUS_3$ shows M–Q orbital overlap in the valence band and U–Q orbital overlap in the conduction band. Periodic DFT spin band-structure calculations on those same compounds establish two energetically similar antiferromagnetic spin structures and show magnetic interactions within and between the layers of the structure. Magnetic susceptibility data for $RbAuUSe_3$,[35] which yield a large negative Weiss constant ($-3.5(2) \times 10^2$ K), are consistent with this hypothesis. The measured effective magnetic moment (μ_{eff} = 3.81(9) μ_B) of $RbAuUSe_3$ suggests that the oxidation state of U is +IV.

2.3.5 AAn_2Q_6[38-40]. In our laboratory the compounds AAn_2Q_6 were synthesized by the reaction of An metal (or β-US_2 in the case of $K_{0.91}U_{1.79}S_6$) in an A_2Q_x flux at temperatures ranging from 873 to 1273 K. These layered materials crystallize in one of two space groups (Table 4 and Fig. 12), either *Immm* in the KTh_2Se_6 structure type[41] or *Cmcm* in the $CsTh_2Te_6$ structure type (2.8.3).[42] The difference between the two structure types is that in the *Cmcm* structure, each AnQ_3 layer is shifted by 1/2*a*, whereas each layer in the *Immm* structure is shifted by 1/2(*a* + *b*). The two structure types can be visualized as intercalation of an A^+ cation into the corresponding AnQ_3 structure. In other words, the structure comprises $^2_\infty[An_2Q_6^-]$ layers alternating with A^+ cations stacked in the [010] direction (*Cmcm*) or the [001] direction (*Immm*). Each A atom is coordinated in a square-prismatic site of Q atoms. These layers contain An atoms coordinated by eight Q atoms in a bicapped trigonal-prismatic geometry.

All the compounds contain Q–Q interactions. In the sulfide compounds, there are S_2^{2-} disulfide anions, whereas in the Te compounds there are infinite Te–Te chains. In the Se compounds, the behavior is intermediate between Se_2^{2-} diselenide anions and infinite Se–Se chains. Only in the sulfides is it apparent how to assign formal oxidation states to An. The selenides contain alternating short and long Se–Se distances, but both are at least 0.4 Å longer than a normal Se–Se bond. An infinite linear chain of equally spaced Te (or other p-block) elements in theory should distort. Electron diffraction studies on KTh_2Se_6 and $RbTh_2Se_6$[41] reveal 4*a* × 4*b* superstructures. The structures, as determined by conventional X-ray diffraction methods, would therefore average any distortions in the Q–Q bonding. The existence of superstructure in other members of the family is certainly a possibility. The elucidation of the fine details of any distortions in these structures is now more feasible than it was a decade ago because X-ray diffraction methods are much more sensitive and the software for handling modulated structures has improved immensely.

Table 4 Known compounds in the AAn_2Q_6 family

Compound	Structure type
KTh_2Se_6[b]	*Immm*
$RbTh_2Se_6$[b]	*Immm*
$CsTh_2Se_6$[a,c]	*Immm*
KTh_2Te_6[a]	*Cmcm*
$CsTh_2Te_6$[d]	*Cmcm*
$K_{0.91}U_{1.79}S_6$[e]	*Immm*
$Rb_{0.85}U_{1.74}S_6$[c]	*Immm*
KU_2Se_6[e,f]	*Immm*
TlU_2Se_6[c]	*Immm*
RbU_2Se_6[c]	*Immm*
CsU_2Se_6[f]	*Immm*
$Cs_{0.88}(La_{0.68}U_{1.32})Se_6$[c]	*Immm*
$Tl_{1.12}U_2Te_6$[g]	*Cmcm*
KNp_2Se_6[c]	*Immm*
$CsNp_2Se_6$[c]	*Immm*

[a] Ref. 38. [b] Ref. 41. [c] Ref. 40. [d] Ref. 42. [e] Ref. 39. [f] Ref. 85. [g] Ref. 86.

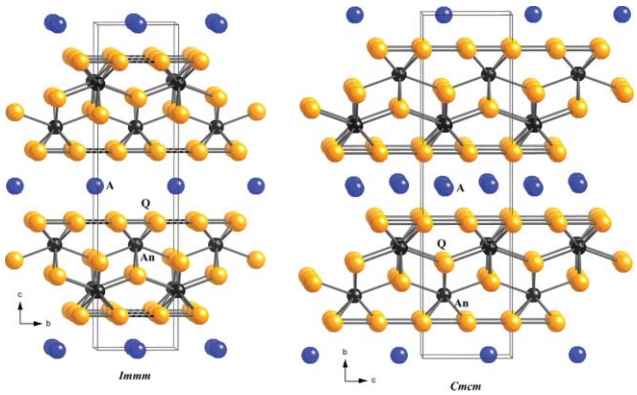

Fig. 12 Comparison of the unit cells of the KTh_2Se_6 structure type (space group *Immm*) and the $CsTh_2Te_6$ structure type (space group *Cmcm*), both viewed down [100].

Only a limited number of physical measurements have been performed on these compounds. The electrical conductivities of KTh_2Se_6,[41] $CsTh_2Se_6$,[40] and KTh_2Te_6[38] are each below 1 × 10^{-5} S cm^{-1} at both 77 K and 298 K. KU_2Se_6[38] and RbU_2Se_6[39] are weak semiconductors, with σ_{298} equal to 1 × 10^{-3} S cm^{-1} and 6 × 10^{-5} S cm^{-1}, respectively. When fit to the Curie–Weiss law, the magnetic susceptibility data for KU_2Se_6 and RbU_2Se_6 yield the following values for *C*, θ, and μ_{eff}: 2.17(1) emu K mol^{-1} and 1.76(1) emu K mol^{-1}, –81.2(6) K and –64(1) K, 2.95(1) μ_B/U and 2.651(8) μ_B/U. The diffuse reflectance spectrum for KU_2Se_6 reveals f–f transitions, and allows a band gap between 0.4 and 0.8 eV to be estimated.

2.3.6 $Cs_2Hg_2USe_5$[43]. The compound $Cs_2Hg_2USe_5$ was obtained in about 25% yield from the solid-state reaction of U, HgSe, Cs_2Se_3, Se, and CsI at 1123 K. This material crystallizes in a new structure type in space group *P*2/*n*. The structure (Fig. 13) contains $^2_\infty[Hg_2USe_5^{2-}]$ layers separated by Cs^+ cations. Within the layers are distorted $HgSe_4$ tetrahedra and regular USe_6 octahedra. In the temperature range 25 to 300 K $Cs_2Hg_2USe_5$ displays Curie–Weiss paramagnetism with μ_{eff} = 3.71(2) μ_B. The compound exhibits semiconducting behavior in the [010] direction; the conductivity at 298 K is 3 × 10^{-3} S cm^{-1}. Formal oxidation states of Cs/Hg/U/Se may be assigned as +I/+II/+IV/–II, respectively.

2.3.7 $Rb_6Cu_{12}U_2S_{15}$[44]. The compound $Rb_6Cu_{12}U_2S_{15}$ was synthesized from the reaction of U, Cu, Rb_2S_3, and S at 793 K. If

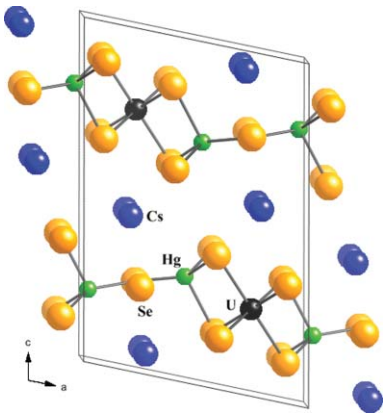

Fig. 13 Unit cell of $Cs_2Hg_2USe_5$ as viewed approximately along [010].

a higher temperature (873 K) or a lesser amount of Cu and S are used then RbCuUS$_3$ (2.3.4) is produced. $Rb_6Cu_{12}U_2S_{15}$ crystallizes in space group $Ia\bar{3}d$ and is isostructural with $K_6Cu_{12}U_2S_{15}$.[45] Its three-dimensional structure is constructed from US$_6$ octahedra interconnected through CuS$_3$ trigonal planar units (Fig. 14). Viewed parallel to the *a*-axis of the structure, small channels hosting Rb atoms are apparent.

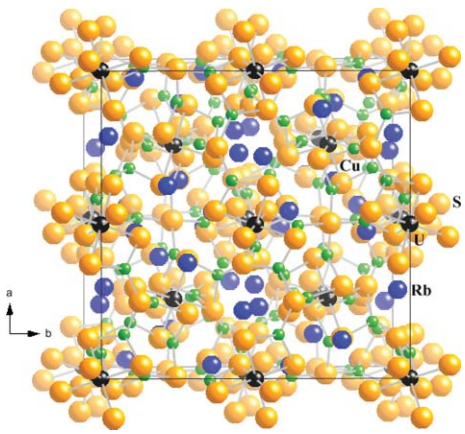

Fig. 14 Unit cell of $Rb_6Cu_{12}U_2S_{15}$ as viewed down [001].

The oxidation state of U is puzzling for these isostructural compounds. If they contain U in the +VI oxidation state and Cu in the +I oxidation state then they are charge balanced and should be semiconductors. They should also be diamagnetic. However, measurements of the electrical conductivity of a polycrystalline sample of $K_6Cu_{12}U_2S_{15}$ were consistent with metallic behavior. Yet, electrical conductivity measurements on a single crystal of $Rb_6Cu_{12}U_2S_{15}$ show that it has very high resistance. Magnetic susceptibility measurements on a powder sample of $K_6Cu_{12}U_2S_{15}$ show Curie–Weiss behavior in the temperature range 100–300 K and μ_{eff} ~2.1 μ_B, which is relatively close to the calculated free-ion value for U^{5+} (2.54 μ_B). Similar measurements on crushed single crystals of $Rb_6Cu_{12}U_2S_{15}$ give μ_{eff} ~0.6 μ_B. Bond-valence sum calculations for the U atoms in both compounds are consistent with U(V). If the compound contains U(V), then charge balance and metallic behavior could be achieved with the presence of oxidized S^{1-} radical anions, as in CuS, which also contains formally oxidized S^{1-} radical anions [*i.e.* $(Cu^+)_3(S_2^{2-})(S^{1-})$].[87]

2.4 Compounds synthesized from alkali-metal or alkaline-earth-metal halide fluxes

The alkali-metal and alkaline-earth-metal halide (F, Cl, Br, I) salts can assume several roles in the synthesis and crystallization of new solid-state compounds. At temperatures below the melting points of the halide salts, they can act as nucleation points for the crystallization of the product. When the temperature of the reaction is raised above the melting point of the halide salt, the salt can also serve as a molten reaction medium,[46] similar to that formed from alkali-metal polychalcogenides. The melting points of the halide salts are typically higher than those of the alkali-metal polychalcogenides, but lower than the elements (transition-metals, lanthanides, actinides) themselves. The melting points for all of the alkali-metal and alkaline-earth-metal halide salts are known[47] and range from a low of 723 K (LiI) to a high of 1723 K (SrF_2). Multiple halide salts can be combined to form eutectic mixtures with melting points lower than those of the individual constituents. The alkali-metal and alkaline-earth-metal halide salts function as either reactive or non-reactive fluxes. It is difficult to predict *a priori* whether the flux will be reactive or not.

Halide salts can be used in open or closed systems, depending on the reactivity and stability of the other reactants. In closed systems involving reactions in fused-silica tubes, precautions must be taken at temperatures above the melting points of the halide salts. Similar to the alkali-metal polychalcogenides, halide salts can react with the tube to scavenge silicon or oxygen or both, as well as potentially etch the tube to the point of rupture. Therefore, it is extremely important that the fused-silica tubes be carbon-coated prior to the reaction. At the conclusion of the reaction, the intended product can be isolated by dissolving the excess halide salt in a solvent such as de-ionized water, acetone, or ethanol.

2.4.1 $MnUSe_3$[48]. $MnUSe_3$ was obtained in about 50% yield from the reaction of the elements in a KBr flux at 1273 K. The compound crystallizes in the $FeUS_3$ structure type (2.1.2 and Fig. 2).

2.4.2 $Cu_{0.78}U_2Te_6$[49]. This compound was synthesized as the major product at 1123 K from the reaction of the elements in a KI flux. It is isostructural with $CuTh_2Te_6$ (2.1.1 and Fig. 1).

2.4.3 $Ba_2Cu_2US_5$[50]. The alkaline-earth uranium chalcogenide $Ba_2Cu_2US_5$ was obtained in a two-step reaction from BaS, Cu_2S, and US_2. In the first step, a mixture of US_2 (prepared from the stoichiometric reaction of U and S at 1223 K) and Cu_2S were reacted at 1323 K. In the second step, that product was ground together with BaS and NaBr (to aid in crystal growth) and reacted at 1123 K. Single crystals were obtained. A rational stoichiometric reaction of BaS, Cu_2S, and US_2 afforded pure powder but no single crystals. This is not an unusual situation. $Ba_2Cu_2US_5$ crystallizes in a new structure type in space group $C2/m$ (Fig. 15). The structure consists of $^2_\infty[Cu_2US_5^{4-}]$ layers separated by Ba^{2+} cations in bicapped trigonal-prismatic coordination. The two-dimensional $^2_\infty[Cu_2US_5^{4-}]$ layer is built from US$_6$ octahedra and CuS$_4$ tetrahedra. A value of μ_{eff} of 2.69(2) μ_B/U was obtained from magnetic susceptibility measurements on the powder. No magnetic transition was observed down to 2 K.

2.4.4 $KCuUS_3$[34]. The compound $KCuUS_3$ was obtained in an exploration of a quinternary system also containing Ca.

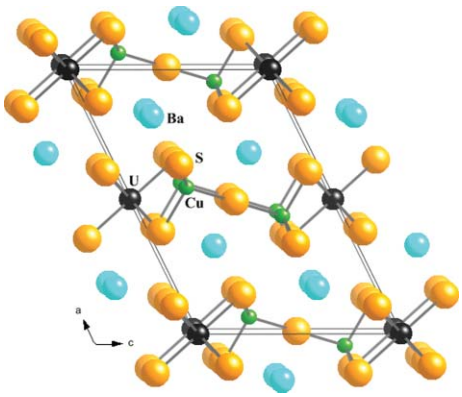

Fig. 15 Unit cell of $Ba_2Cu_2U_2S_5$ as viewed along [010].

Initially, US_2 and Cu_2S were ground together and reacted at 1273 K. The contents of the tube were then ground together with CaS and KBr, and reacted at 1123 K to afford black needles of $KCuUS_3$ in about 10% yield. $KCuUS_3$ crystallizes in the $KCuZrS_3$ structure type (2.3.4, Fig. 11, and Table 3).

2.4.5 $CsAuUTe_3$[35]. Long black single crystals were prepared in about 15% yield from the reaction at 1173 K of U, Au, and Te in a CsCl flux. The compound crystallizes in the $KCuZrS_3$ structure type (2.3.4, Fig. 11, and Table 3).

2.4.6 $Ba_8Hg_3U_3S_{18}$[51]. The compound $Ba_8Hg_3U_3S_{18}$ was obtained in low yield from the reaction of U, HgS, BaS, and S with a $BaBr_2$/KBr eutectic salt flux (mp = 883 K).[52] A more rational stoichiometric reaction of U, HgS, BaS, and S in a $BaCl_2$ salt flux increased the yield to approximately 15%. $Ba_8Hg_3U_3S_{18}$ crystallizes in a new structure type in space group $P\bar{6}$ (Fig. 16). The structure consists of edge-sharing US_6 octahedra that form infinite $^1_\infty[US_4]$ chains, as well as discrete, nearly linear $[S–Hg–S]^{2-}$ dithiomercurate(II) anions. Separating these structural features are Ba atoms in mono- and bicapped trigonal-prismatic arrangements of S atoms.

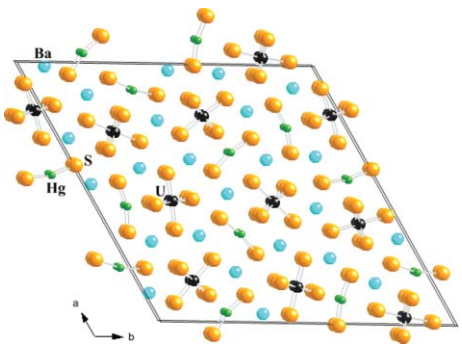

Fig. 16 Unit cell of $Ba_8Hg_3U_3S_{18}$ as viewed down [001].

$Ba_8Hg_3U_3S_{18}$ has an antiferromagnetic transition at T_N = 59 K. Above 100 K, this compound obeys the Curie–Weiss law with the values C = 3.65(5) emu K mol^{-1}, θ = –60(3) K, and μ_{eff} = 3.12(2) μ_B/U. The magnetic data, along with the U–S bond distances, leave the formal oxidation state for U in doubt.

2.4.7 $Cs_{0.88}(La_{0.68}U_{1.32})Se_6$[40]. This compound was synthesized as the major product from the reaction of the elements in a CsCl flux at 1123 K. It belongs to the KTh_2Se_6 structure type (2.3.5, Fig. 12, and Table 4) with both La and U disordered over the same crystallographic site.

2.5 Compounds synthesized with antimony chalcogenide fluxes

Although the use of excess antimony is well-known for the synthesis of Sb-containing intermetallics, less explored has been the use of binary antimony chalcogenides, Sb_2Q_3 (Q = S, Se).[53] These compounds have intermediate melting points (823 K and 884 K, respectively[47]), as well as a tendency not to be incorporated into the final product. Additionally, they form long black columnar crystals that are usually easy to separate mechanically from the desired product. These attributes make antimony chalcogenides useful alternatives to alkali-metal polychalcogenides for the synthesis and crystallization of chalcogen-containing materials.

Antimony chalcogenides can be utilized for both the syntheses of new compounds from the elements or binaries, as well as for the crystallization of compounds from phase-pure powders. Because the antimony chalcogenides are used in conjunction with sulfur or selenium, the reactions must be carried out in sealed vessels. Fortunately, the antimony chalcogenides are sufficiently unreactive so that they can be used in fused-silica tubes that are not carbon-coated.

2.5.1 $Y_4UO_3S_5$[54]. Red needles of $Y_4UO_3S_5$ have been synthesized in about 10% yield by the solid-state reaction at 1273 K of UOS and Y_2S_3 with Sb_2S_3 as a flux. $Y_4UO_3S_5$ crystallizes in space group *Pnma*. It adopts a three-dimensional structure (Fig. 17) that contains five crystallographically unique heavy-atom positions. U and Y atoms disorder on one eight-coordinate metal position bonded to four O atoms and four S atoms and two seven-coordinate metal positions bonded to three O atoms and four S atoms. Another eight-coordinate metal position with two O atoms and six S atoms and one six-coordinate metal position with six S atoms are exclusively occupied by Y atoms. $Y_4UO_3S_5$ is a modified Curie–Weiss paramagnet between 1.8 and 300 K. Its effective magnetic moment is 3.3(2) μ_B. $Y_4UO_3S_5$ has a band gap of 1.95 eV. The electrical resistivity along the [100] direction of a single crystal shows Arrhenius-type thermal activation with an activation energy of 0.2 eV.

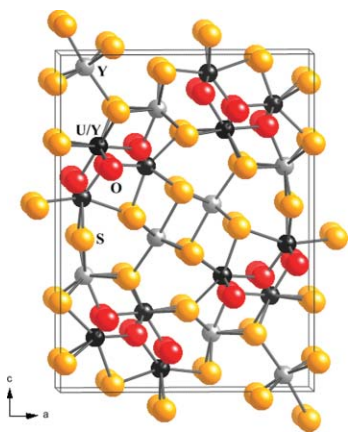

Fig. 17 Unit cell of $Y_4UO_3S_5$ as viewed along [010].

2.5.2 $Yb_2UO_2S_3$ and $Y_2UO_2S_3$[55]. Dark-red square plates of the previously reported compounds "$(UO)_2LnS_3$" (Ln = Yb, Y),

allegedly containing $U^{+3.5}$,[56] have been synthesized by solid-state reactions of UOS and YbS or Y_2S_3 with Sb_2S_3 as a flux at 1273 K. The compounds crystallize in space group *I*4/*mmm*. These isostructural compounds were reinvestigated by single-crystal X-ray diffraction methods. The actual formula of "$(UO)_2LnS_3$" (Ln = Yb, Y) is $(U_{0.5}Ln_{0.5}O)_2LnS_3$, that is $Ln_2UO_2S_3$, which can be charge-balanced with U(IV) and Ln(III). The layered structure (Fig. 18) comprises $(U/Ln)O_4S_4$ square antiprisms alternating with LnS_6 octahedra. U and Ln(1) atoms disorder on the eight-coordinate metal position but Ln(2) atoms occupy the six-coordinate metal position exclusively. $Yb_2UO_2S_3$ is a modified Curie–Weiss paramagnet between 32 and 293 K, below which part of the paramagnetic moments go through a possible ferromagnetic transition. The band gaps of $Ln_2UO_2S_3$ (Ln = Yb, Y) are around 2 eV.

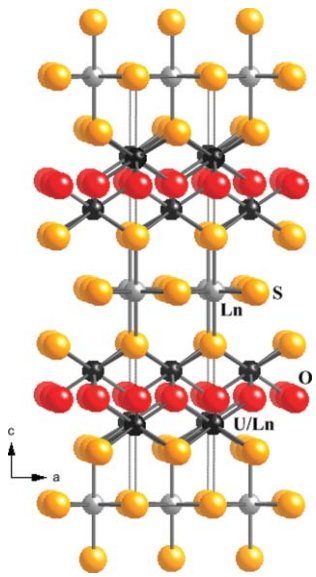

Fig. 18 Unit cell of $Ln_2UO_2S_3$ (Ln = Yb, Y) as viewed down [010].

2.5.3 $La_2U_2Se_9$[57]. The compound $La_2U_2Se_9$ was obtained in high yield from the stoichiometric reaction of the elements in an Sb_2Se_3 flux at 1123 K. The compound, which crystallizes in a new structure type (Fig. 19) in space group *Pmma*, has a three-dimensional structure with alternating U/Se and La/Se layers attached by three independent, infinite polyselenide chains. The Se coordination about the U atom is monocapped square-antiprismatic, whereas about one La atom it is bicapped square-prismatic and about the other La atom it is trigonal-prismatic. $La_2U_2Se_9$ is the first example of an ordered lanthanide/actinide chalcogenide with a novel structure type.

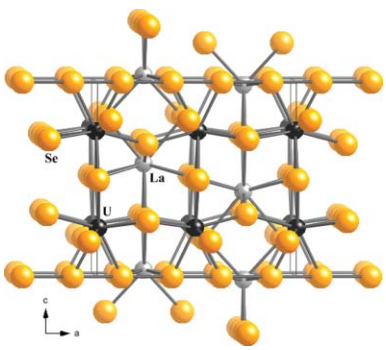

Fig. 19 Unit cell of $La_2U_2Se_9$ as viewed along [010].

$La_2U_2Se_9$ displays an antiferromagnetic transition at $T_N = 5$ K; above 50 K, the paramagnetic behavior can be fit to the Curie–Weiss law to yield a μ_{eff} of 3.10(1) μ_B/U. The low-temperature specific heat of $La_2U_2Se_9$ exhibits no anomalous behavior near the Néel temperature that might indicate long-range magnetic ordering or a phase transition. XANES spectra confirm the assignment of formal oxidation states as La(III) and U(IV).

2.6 Compounds synthesized with a tin flux

Tin flux[58] has been widely used for the syntheses of pnictides, borides, and silicides, as well as Sn-containing intermetallics.[59] Much rarer are examples of Sn being used as a flux for the synthesis and crystallization of chalcogenides. The effectiveness of Sn metal as a flux results in part from its low melting point of 505 K;[47] in fact, the only d- or p-block metals with lower melting points are Hg, Ga, and In. Whether or not Sn is incorporated into the final product depends upon the relative thermodynamic stabilities of the chalcogenide *versus* that of the corresponding stannide.

Reactions with a Sn flux are typically carried out in sealed vessels. When Sn is not incorporated into the final product it often forms metallic droplets that can be manually separated from the crystalline product. Other methods of isolating the product include hot centrifugation while the Sn is still molten, or soaking the Sn-rich matrix in dilute HCl.

2.6.1 $SrTh_2Se_5$[15]. $SrTh_2Se_5$ was formed from the reaction of Th, SrSe, Se, and Sn (in the ratio 1 : 1 : 3 : 3) at 1273 K. A few crystals of $SrTh_2Se_5$ grew as transparent red blocks; they were manually extracted from the reaction mixture. Attempts to synthesize $SrTh_2Se_5$ by a stoichiometric reaction of the elements proved unsuccessful. $SrTh_2Se_5$ crystallizes in space group $P2_1/c$ with a structure (Fig. 20) derived from the U_3S_5 structure type.[60] U_3S_5 can be rationalized as $(U^{3+})_2(U^{4+})(S^{2-})$, whereas in $SrTh_2Se_5$ one U(III) is replaced by Sr(II), and the other U(III) is "oxidized" to Th(IV).

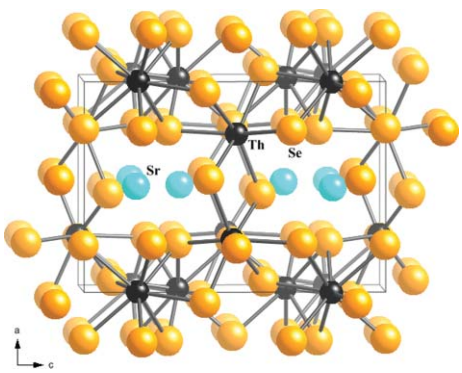

Fig. 20 Unit cell of $SrTh_2Se_5$ as viewed down [010].

There are two independent Th atoms in $SrTh_2Se_5$. Atom Th(1) is coordinated to eight Se atoms in a bicapped trigonal prism whereas atom Th(2) is coordinated to seven Se atoms in a highly distorted face-capped octahedron. Each Th(1) atom shares all three edges of the trigonal prism with three Th(1) neighbors; two of the neighboring atoms share caps as well. Connected in

this way the Th(1) atoms form a $^{2}_{\infty}[ThSe_8^{4-}]$ net perpendicular to [100], and Th(2) atoms form chains of edge-shared octahedra that run perpendicular to the $^{2}_{\infty}[ThSe_8^{4-}]$ layer through the holes of the net. The overall structure is three-dimensional with Sr^{2+} cations situated in one-dimensional channels along [010]. Each Sr atom is coordinated to eight Se atoms in a bicapped trigonal prism.

2.6.2 $MnThSe_3$[16] and $MgThTe_3$[48]. Crystals of $MnThSe_3$ were synthesized in low yield from stoichiometric amounts of Th, Mn, and Se with Sn as a flux at 1223 K. The compound $MgThTe_3$ has been synthesized in almost 100% yield as small black plates from the stoichiometric reaction of the elements with Sn as a flux at 1173 K. Both compounds crystallize in the $FeUS_3$ structure type (2.1.2 and Fig. 2).

2.7 Compound synthesized through a metathesis reaction

Metathesis reactions involve the exchange of anions between alkali-metal oxides, chalcogenides, or pnictides and one or more metal halides.[61] If the alkali-metal compound is used in excess, rather than stoichiometrically, then the alkali-metal may be incorporated into the final product. The formation of the alkali-metal halide salt is a thermodynamic driving force (owing to its extreme stability). The resultant alkali-metal halide salt can serve as a reaction medium or aid in the crystallization of the desired product (2.4). The actual metathesis reaction is very exothermic and occurs rapidly at the initiation temperature. Thus, in most instances a powder is formed. It is sometimes possible to obtain single crystals by annealing the powder at a higher temperature followed by prolonged slow cooling.

Because of the energy-intensive nature of a metathesis reaction, it must be performed in a sealed vessel. If it is carried out in a fused-silica tube, the tube must be carbon-coated or else the exothermic reaction and resulting molten salt will instantly rupture the tube. Upon completion of the reaction, the excess halide salt can be dissolved in an appropriate solvent to leave the desired product behind.

2.7.1 $K_2Cu_3US_5$[62]. The initial reaction, consisting of UCl_4, CuCl, and K_2S in the ratio 1 : 2 : 3, involved prolonged heating at 623 K, next at 973 K, and then slow cooling. The compound $K_2Cu_3US_5$ crystallized as black needles and plates. Once the composition was established, a more rational synthesis was found. This proceeded from the reaction mixture of UCl_4, CuCl, K_2S, and S in the ratio 1 : 3 : 5 : 4. This mixture was subjected to the same heating cycle as the initial one to afford crystals of $K_2Cu_3US_5$ in about 25% yield.

$K_2Cu_3US_5$ crystallizes in a new structure type in space group *Cmcm* (Fig. 21). The structure comprises $^{2}_{\infty}[Cu_3US_5^{2-}]$ slabs separated by K^+ cations. The slabs are built from CuS_4 tetrahedra and US_6 octahedra. In the temperature range 130 to 300 K the compound exhibits Curie–Weiss magnetic behavior with $\mu_{eff} = 2.45(8)\ \mu_B$. This result together with both bond distances, bond valence calculations, and the absence of a Cu(II) ESR signal support the formulation of this compound as $(K^+)_2(Cu^+)_3(U^{5+})(S^{2-})_5$. A formal oxidation state of +V for U is rare.

2.8 Compounds synthesized serendipitously

In addition to the science inherent in the syntheses of solid-state compounds, some degree of luck is necessary for success (1).

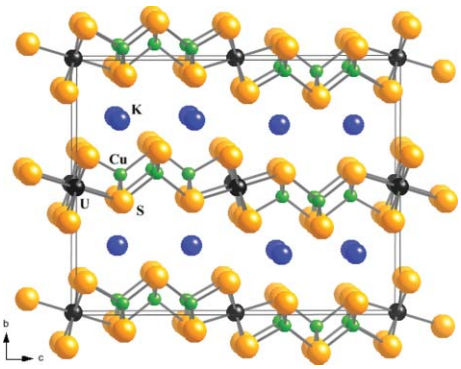

Fig. 21 Unit cell of $K_2Cu_3US_5$ as viewed along [100].

It is difficult, if not impossible, to predict beforehand with any certainty what the products of a given solid-state reaction will be. The serendipitous results of solid-state synthetic chemistry can be divided into two categories. In one, the final product contains elements not found in the starting materials. Examples of this include silicon or oxygen scavenged from fused-silica tubes, metals incorporated from inert containment vessels, or unknown impurities in allegedly pure commercial reactants. (We add, parenthetically, that in solid-state syntheses it is prudent to confirm the compositions of all starting materials.) In the other category, a certain element or compound may not be incorporated into the final product, yet its presence is necessary for the product formation (or else for better yield from an otherwise low-yield reaction). These various unquantifiable variables contribute to the art and joy of solid-state synthetic chemistry.

2.8.1 UOSe[63]. A single crystal of UOSe was discovered in the products of the reaction of K_2Se, Cu, U, and Se at 1223 K. The target was the U analogue of $KCuZrSe_3$. Oxygen is presumed to have been extracted from the fused-silica tube. UOSe crystallizes in space group *P4/nmm* in the PbFCl structure type.[64] The structure (Fig. 22) contains a nine-coordinate U atom bonded to five Se atoms and four O atoms in a distorted tricapped trigonal-prismatic arrangement.

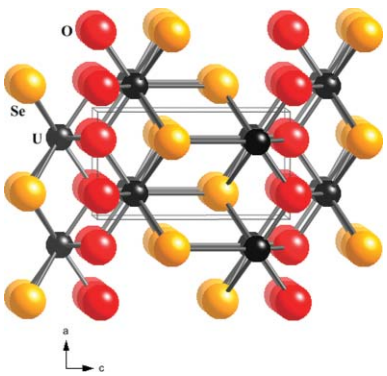

Fig. 22 Unit cell of UOSe as viewed down [010].

2.8.2 $CsTh_2Te_6$[42]. In an attempt to prepare $CsHfThTe_5$, the Th/Hf analogue of $CsTiUTe_5$ (2.3.2), $CsTh_2Te_6$ was prepared instead. The elements Th, Hf, and Te were combined with Cs_2Te_3 and reacted at 1073 K. A few lustrous, black crystals formed at the surface and within uncharacterized, amorphous byproducts.

$CsTh_2Te_6$ crystallizes in space group *Cmcm* in a new structure type, as described in 2.3.5 (Fig. 12, and Table 4). The electrical conductivity of this compound is less than 1×10^{-5} S cm^{-1} at 295 K.

2.8.3 US_3[65]. The compound US_3 was obtained as black plates from a solid-state reaction of Cs_2S_3, UCl_4, and AgCl, the target being the Ag analogue of $K_2Cu_3US_5$ (2.7.1). The sample was kept at 523 K, then 923 K, and finally slow cooled. US_3 was obtained in about 10% yield. Previously, this compound had only been characterized by powder X-ray diffraction methods.[66,67] US_3 crystallizes in space group $P2_1/m$ in the TiS_3 structure type (Fig. 23).[68] The structure consists of two-dimensional layers that stack perpendicular to [001]. Each layer comprises US_8 bicapped trigonal prisms that edge-share in the [100] direction and face-share in the [010] direction. The compound may be described as $(U^{4+})(S^{2-})(S_2^{2-})$.

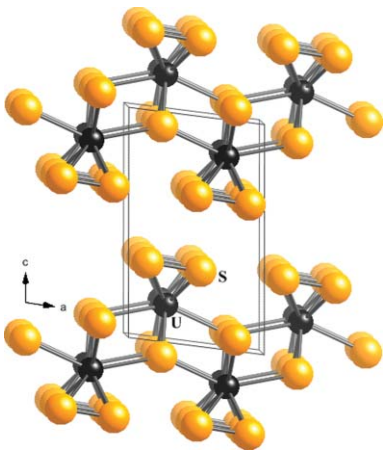

Fig. 23 Unit cell of US_3 as viewed along [010].

2.8.4 $Cu_{0.60}USb_2$[69]. A few single crystals of $Cu_{0.60(4)}USb_2$, were obtained from the reaction of USb_2 and CuO at 1173 K. The target was a U/Sb/O/S compound. $Cu_{0.60(4)}USb_2$ crystallizes in the $HfCuSi_2$ structure type[70] in space group $P4/nmm$. Zigzag USb sheets stack perpendicular to [001] (Fig. 24). These sheets are separated by square-planar nets of Sb atoms and Cu atoms. The U atoms are surrounded by a square antiprism of Sb atoms. The geometry around one unique Sb atom is a square antiprism of Cu and U atoms; around the other unique Sb atom it is a tetrahedron of U atoms. Cu atoms are tetrahedrally coordinated to four Sb atoms. Other members of the Cu_xUSb_2 family of compounds include $Cu_{0.44}USb_2$,[71] $Cu_{0.83}USb_2$,[72] and $CuUSb_2$.[73] These compounds obey Vegard's law in that the cell constant *c* increases linearly with Cu occupancy.

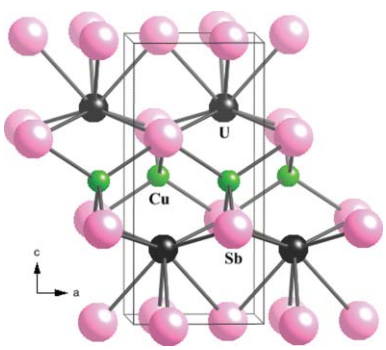

Fig. 24 Unit cell of $Cu_{0.60}USb_2$ as viewed down [010].

2.8.5 $Ba_4Cr_2US_9$[74]. Black needles of $Ba_4Cr_2US_9$ were first found accidentally in a two-step reaction that involved BaS, Cu_2S, and US_2. It turned out that Cr was an impurity in this reaction. The source of Cr was probably from contamination of the vacuum line from loadings of previous reactions. A powder of $Ba_4Cr_2US_9$ was obtained in a rational manner from the stoichiometric reaction of BaS, Cr_2S_3, and US_2 at 1323 K, but single crystals could not be prepared by this technique.

$Ba_4Cr_2US_9$ crystallizes in space group *P*321. The structure (Fig. 25) consists of one-dimensional $^1_\infty[Cr_2US_9^{8-}]$ chains separated by Ba^{2+} cations. There are two crystallographically unique one-dimensional chains each composed of face-sharing CrS_6 octahedra and US_6 trigonal prisms in the sequence *oct oct tp oct oct tp* with the U and Cr cations in a linear arrangement parallel to [001]. There are no S–S bonds in the structure so formal oxidation states of +II, +III, +IV, and –II may be assigned to Ba, Cr, U, and S, respectively.

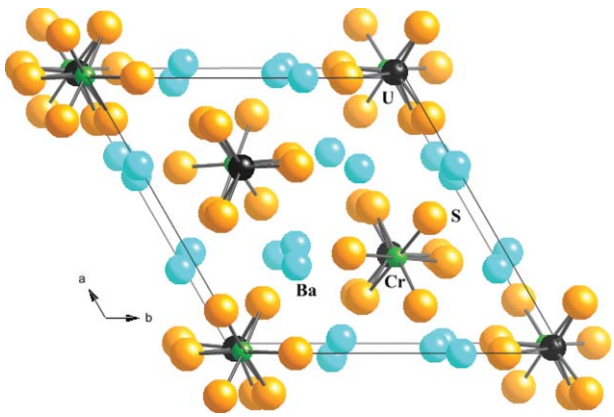

Fig. 25 Unit cell of $Ba_4Cr_2US_9$ as viewed along [001].

2.8.6 $Ta_2UO(S_2)_3Cl_6$[75]. This compound was synthesized from UCl_4 and TaS_2 at 883 K. The product consisted of small orange needles of what turned out to be $Ta_2UO(S_2)_3Cl_6$ in approximately 40% yield. The reaction tube was not etched. Therefore, the fused silica was not the source of O in $Ta_2UO(S_2)_3Cl_6$. The actual source was presumably the "old lot" of TaS_2, with which the compound could be synthesized repeatedly in good yield. The compound could not be obtained when a "new lot" of TaS_2 was used as a reactant. X-Ray powder patterns of the old and new lots indicate that both contain a variety of TaS_2 polymorphs. Unfortunately, there are no single crystal data on TaO_xS_{2-x} compounds from which to calculate X-ray diffraction powder patterns.

The compound $Ta_2UO(S_2)_3Cl_6$ crystallizes in the space group $P\bar{1}$. Its structure (Fig. 26) comprises a UTa_2 unit bridged by μ_2-S_2 and μ_3-O groups. Each Ta atom bonds to two μ_2-S_2, the μ_3-O, and two terminal Cl atoms. Each U atom bonds to two μ_2-S_2, the μ_3-O, and four Cl atoms. The Cl atoms bridge in pairs to neighboring U atoms to form a ribbon structure. The bond distances are normal and are consistent with formal oxidation

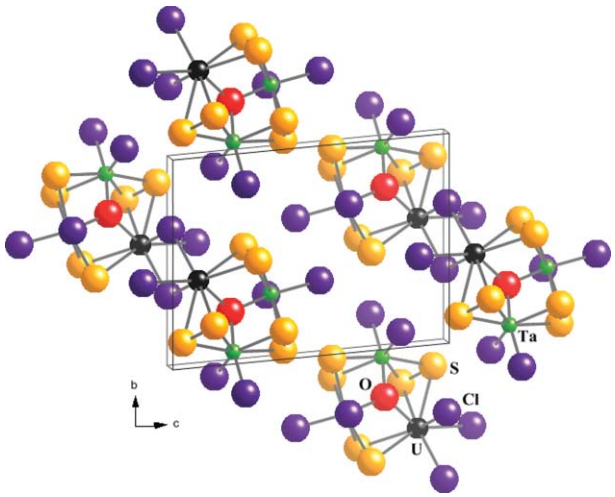

Fig. 26 Unit cell of $Ta_2UOS_6Cl_6$ as viewed down a^*.

states of +V/+IV/–II/–I/–I for Ta/U/O/S/Cl, respectively. The optical absorbance spectrum of $Ta_2UO(S_2)_3Cl_6$ displays characteristic transition peaks near the absorption edge. Density functional theory was used to assign these peaks to transitions between S^{1-} valence-band states and empty U 5f–6d hybrid bands. Density-of-states analysis shows overlap between Ta 5d and U bands, consistent with metal–metal interactions.

2.8.7 TlU_2Se_6[40]. In an attempt to prepare $Tl_2Hg_2USe_5$, the Tl analogue of $Cs_2Hg_2USe_5$ (2.3.6), TlU_2Se_6 was synthesized instead. Elemental U and Se were reacted with HgSe and Tl_2Se at 1073 K. A low yield of golden black plates of TlU_2Se_6 was found. TlU_2Se_6 crystallizes in the KTh_2Se_6 structure type (2.3.5, Fig. 12, and Table 4).

2.8.8 $CsTi_5Te_8$[76]. The compound $CsTi_5Te_8$ was obtained as a crystalline product by a "U-assisted" reaction of Cs, Ti, U, and Cs_2Te_3 in a CsCl flux at 1173 K. The material crystallizes in space group $I2/m$. The structure of $CsTi_5Te_8$ (Fig. 27) contains a three-dimensional network of face-sharing and edge-sharing $TiTe_6$ octahedra that form one-dimensional channels. The Cs^+ cations reside in channels that propagate in the [010] direction. The structure is closely related to several other types of channel

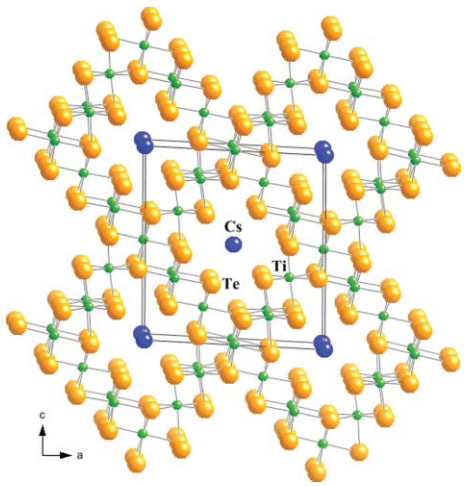

Fig. 27 Unit cell of $CsTi_5Te_8$ as viewed along [010].

structures, including those of the minerals of the hollandite and psilomelane families, and those with the TlV_5S_8[77] and $TlCr_3S_5$[78] structure types. Attempts to obtain the compound in a rational manner, in particular in the absence of U, were unsuccessful.

2.8.9 $Ba_4Fe_2I_5S_4$[79]. The compound $Ba_4Fe_2I_5S_4$ has been prepared at 1173 K by the "U-assisted" reaction of FeS, BaS, S, and U with BaI_2 as a flux. A more rational synthesis was found; however, the presence of U appears to be essential for the formation of single crystals suitable for X-ray diffraction studies. $Ba_4Fe_2I_5S_4$ crystallizes in a new structure type in space group $I4/m$. The structure (Fig. 28) consists of a Ba–I network penetrated by $^1_\infty[Fe_2S_4]$ chains. Each Fe atom is tetrahedrally coordinated to four S atoms. The FeS_4 tetrahedra edge share to form linear $^1_\infty[Fe_2S_4]$ chains in the [001] direction. The Fe–Fe interatomic distance in these chains is 2.5630(4) Å, only about 3% longer than the shortest Fe–Fe distance in α-Fe metal. Charge balance dictates that the average formal oxidation state of Fe in these chains be +2.5.

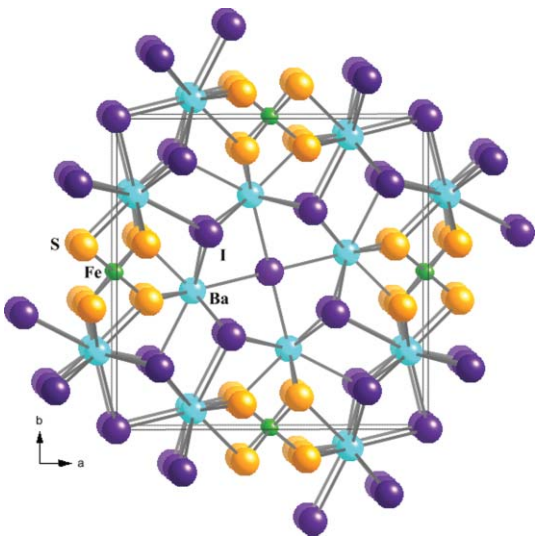

Fig. 28 Unit cell of $Ba_4Fe_2I_5S_4$ as viewed down [001].

The Mössbauer spectra obtained at 85 and 270 K comprise a single quadrupole doublet that has hyperfine parameters consistent with an average Fe oxidation state of +2.5. The Mössbauer spectrum obtained at 4.2 K consists of a single magnetic sextet with a small hyperfine field of –15.5 T. This spectrum is also consistent with rapid electron delocalization and an average Fe oxidation state of +2.5. The molar magnetic susceptibility of $Ba_4Fe_2I_5S_4$, obtained between 3.4 and 300 K, qualitatively indicates the presence of weak pseudo-one-dimensional ferromagnetic exchange within a linear chain above 100 K and weak three-dimensional ordering between the chains at lower temperatures.

3. Postscript

In keeping with the topic of this Issue, we have concentrated on synthetic methods and organized this paper accordingly. As a result it may not have been obvious why particular target compounds were chosen. Had we organized the paper by the chemistry involved it would have been clearer that the syntheses of solid-state compounds still involve both science and "art," to return to DiSalvo's caveat. It took several centuries for synthetic

organic chemistry to reach its current level of sophistication. However, the solid-state chemist is confronted by many more elements than is the organic chemist. Progress toward the ultimate goal of designed syntheses of solid-state compounds for specific structures or physical properties is being made, but progress remains very slow. In the interim some of us find it exciting and fun to be engaged in one of the last frontiers of synthetic chemistry.

Acknowledgements

The research described in this Perspective was supported by the U.S. Department of Energy, Basic Energy Sciences, Chemical Sciences, Biosciences, and Geosciences Division and Division of Materials Sciences and Engineering Grant ER-15522. We thank Dr. Lynda Soderholm, Directory of the Actinide Facility, Argonne National Laboratory, for providing facilities for our Np studies. We are indebted to Dr. Dick T. Co for creating the cover image. JAI is deeply indebted to the members of his research group, comprising at various times combinations of undergraduate students, graduate students, postdoctoral fellows, and visitors. Many fruitful collaborations with colleagues, local and international, have enhanced and continue to enhance the research efforts described here. The names of all of these individuals will be found in the Reference section below.

References

1 R. Hoffmann, *Angew. Chem., Int. Ed. Engl.*, 1987, **26**, 846–878.
2 M. G. Kanatzidis and K. R. Poeppelmeier, *Prog. Solid State Chem.*, 2007, **36**, 1–133.
3 Abbreviations used within the text: A = alkali-metal; An = actinide; Ln = lanthanide; M = transition-metal; Q = chalcogenide.
4 H. R. Ott, H. Rudigier, Z. Fisk and J. L. Smith, *Phys. Rev. Lett.*, 1983, **50**, 1595–1598.
5 G. R. Stewart, Z. Fisk, J. O. Willis and J. L. Smith, *Phys. Rev. Lett.*, 1984, **52**, 679–682.
6 C. H. de Novion, D. Damien and H. Hubert, *J. Solid State Chem.*, 1981, **39**, 360–367.
7 D. Damien, C. H. de Novion and J. Gal, *Solid State Commun.*, 1981, **38**, 437–440.
8 J. L. Sarrao, L. A. Morales, J. D. Thompson, B. L. Scott, G. R. Stewart, F. Wastin, J. Rebizant, P. Boulet, E. Colineau and G. H. Lander, *Nature*, 2002, **420**, 297–299.
9 Y. Haga, D. Aoki, Y. Homma, S. Ikeda, T. D. Matsuda, E. Yamamoto, H. Sakai, N. Tateiwa, N. D. Dung, A. Nakamura, Y. Shiokawa and Y. Onuki, *J. Alloys Compd.*, 2008, **464**, 47–50.
10 F. J. DiSalvo, *Science*, 1990, **247**, 649–655.
11 A. J. K. Haneveld and F. Jellinek, *J. Less Common Met.*, 1969, **18**, 123–129.
12 J. A. Hermann and J. F. Suttle, 1957: Uranium(IV) Chloride. In: *Inorganic Synthesis. Vol. 5*. (T. Moeller) McGraw-Hill Book Company, New York, 143–145.
13 I. Grenthe, J. Drozdzynski, T. Fujino, E. C. Buck, T. E. Albrecht-Schmitt and S. F. Wolf, 2006: Uranium in *The Chemistry of the Actinide and Transactinide Elements*. Third ed. Vol. 1. (L. R. Morss, N. M. Edelstein and J. Fuger) Springer, Dordrecht, 253–698.
14 R. C. Larroque, R. Chipaux and M. Beauvy, *J. Less Common Met.*, 1986, **121**, 487–496.
15 A. A. Narducci and J. A. Ibers, *Inorg. Chem.*, 1998, **37**, 3798–3801.
16 A. A. Narducci and J. A. Ibers, *Inorg. Chem.*, 2000, **39**, 688–691.
17 H. Noël and J. Padiou, *Acta Crystallogr., Sect. B: Struct. Crystallogr. Cryst. Chem.*, 1976, **32**, 1593–1595.
18 D. M. Wells and J. A. Ibers, *Z. Anorg,. Allg. Chem.*, 2010, **636**, 440–442.
19 H. Schäfer, *Chemical Transport Reactions*, Academic Press, New York, 1964.
20 D. E. Bugaris and J. A. Ibers, *J. Solid State Chem.*, 2008, **181**, 3189–3193.
21 D. M. Wells, S. Skanthakumar, L. Soderholm and J. A. Ibers, *Acta Crystallogr., Sect. E: Struct. Rep. Online*, 2009, **65**, i14.
22 A. Daoudi, M. Lamire, J. C. Levet and H. Noël, *J. Solid State Chem.*, 1996, **123**, 331–336.
23 M. Julien-Pouzol, S. Jaulmes, A. Mazurier and M. Guittard, *Acta Crystallogr., Sect. B: Struct. Crystallogr. Cryst. Chem.*, 1981, **37**, 1901–1903.
24 D. M. Wells, E. Ringe, D. Kaczorowski, D. Ginda, G. André, R. G. Haire, D. E. Ellis and J. A. Ibers, in preparation.
25 D. Kaczorowski, J. H. Albering, H. Noël and W. Jeitschko, *J. Alloys Compd.*, 1994, **216**, 117–121.
26 V. Johnson and W. Jeitschko, *J. Solid State Chem.*, 1974, **11**, 161–166.
27 R. Troc, J. Leciejewicz and R. Ciszewski, *Phys. Status Solidi*, 1966, **15**, 515–519.
28 R. Troc, *Inorg. Chim. Acta*, 1987, **140**, 67–77.
29 S. A. Sunshine, D. Kang and J. A. Ibers, *J. Am. Chem. Soc.*, 1987, **109**, 6202–6204.
30 M. G. Kanatzidis and Y. Park, *J. Am. Chem. Soc.*, 1989, **111**, 3767–3769.
31 J. A. Cody and J. A. Ibers, *Inorg. Chem.*, 1995, **34**, 3165–3172.
32 J.-Y. Kim, D. L. Gray and J. A. Ibers, *Acta Crystallogr., Sect. E: Struct. Rep. Online*, 2006, **62**, i124–i125.
33 F. Q. Huang, K. Mitchell and J. A. Ibers, *Inorg. Chem.*, 2001, **40**, 5123–5126.
34 J. Yao, D. M. Wells, G. H. Chan, H.-Y. Zeng, D. E. Ellis, R. P. Van Duyne and J. A. Ibers, *Inorg. Chem.*, 2008, **47**, 6873–6879.
35 D. E. Bugaris and J. A. Ibers, *J. Solid State Chem.*, 2009, **182**, 2587–2590.
36 D. M. Wells, G. B. Jin, S. Skanthakumar, R. G. Haire, L. Soderholm and J. A. Ibers, *Inorg. Chem.*, 2009, **48**, 11513–11517.
37 M. F. Mansuetto, P. M. Keane and J. A. Ibers, *J. Solid State Chem.*, 1992, **101**, 257–264.
38 E. J. Wu, M. A. Pell and J. A. Ibers, *J. Alloys Compd.*, 1997, **255**, 106–109.
39 H. Mizoguchi, D. Gray, F. Q. Huang and J. A. Ibers, *Inorg. Chem.*, 2006, **45**, 3307–3311.
40 D. E. Bugaris, D. M. Wells, J. Yao, S. Skanthakumar, R. G. Haire, L. Soderholm and J. A. Ibers, in preparation.
41 K.-S. Choi, R. Patschke, S. J. L. Billinge, M. J. Waner, M. Dantus and M. G. Kanatzidis, *J. Am. Chem. Soc.*, 1998, **120**, 10706–10714.
42 J. A. Cody and J. A. Ibers, *Inorg. Chem.*, 1996, **35**, 3836–3838.
43 D. E. Bugaris, D. M. Wells and J. A. Ibers, *J. Solid State Chem.*, 2009, **182**, 1017–1020.
44 G. B. Jin, J. Yao, D. M. Wells, C. D. Malliakas, M. G. Kanatzidis and J. A. Ibers, in preparation.
45 A. C. Sutorik, R. Patschke, J. Schindler, C. R. Kannewurf and M. G. Kanatzidis, *Chem.–Eur. J.*, 2000, **6**, 1601–1607.
46 D. Elwell, and H. J. Scheel, *Crystal Growth from High-Temperature Solutions*, Academic Press, London, 1975.
47 R. C. Weast, *Handbook of Chemistry and Physics*, The Chemical Rubber Co., Cleveland, 1972.
48 I. Ijjaali, K. Mitchell, F. Q. Huang and J. A. Ibers, *J. Solid State Chem.*, 2004, **177**, 257–261.
49 F. Q. Huang and J. A. Ibers, *J. Solid State Chem.*, 2001, **159**, 186–190.
50 H.-Y. Zeng, J. Yao and J. A. Ibers, *J. Solid State Chem.*, 2008, **181**, 552–555.
51 D. E. Bugaris, D. K. Shuh, and J. A. Ibers, in preparation.
52 R. S. Roth, T. Negas, and L. P. Cook, *Phase Diagrams for Ceramists*, The American Ceramic Society, Columbus, 1983.
53 G. B. Jin, E. S. Choi, R. P. Guertin, J. S. Brooks, C. H. Booth and T. E. Albrecht-Schmitt, *Inorg. Chem.*, 2007, **46**, 9213–9220.
54 G. B. Jin, E. S. Choi, D. M. Wells and J. A. Ibers, *J. Solid State Chem.*, 2009, **182**, 1861–1866.
55 G. B. Jin, E. S. Choi and J. A. Ibers, *Inorg. Chem.*, 2009, **48**, 8227–8232.
56 S. Jaulmes, M. Julien-Pouzoi, M. Guittard, T. Vovan, P. Laruelle and J. Flahaut, *Acta Crystallogr., Sect. C: Cryst. Struct. Commun.*, 1986, **42**, 1109–1111.
57 D. E. Bugaris, R. Copping, T. Tyliszczak, D. K. Shuh and J. A. Ibers, *Inorg. Chem.*, 2010, **49**, 2568–2575.
58 P. Jolibois, *C. R. Chimie*, 1910, **150**, 106–108.
59 M. G. Kanatzidis, R. Pöttgen and W. Jeitschko, *Angew. Chem., Int. Ed.*, 2005, **44**, 6996–7023.
60 M. Potel, R. Brochu, J. Padiou and D. Grandjean, *C. R. Seances Acad. Sci., Ser. C*, 1972, **275**, 1419–1421.
61 I. P. Parkin, *Chem. Soc. Rev.*, 1996, **25**, 199–207.

62 D. L. Gray, L. A. Backus, H.-A. Krug von Nidda, S. Skanthakumar, A. Loidl, L. Soderholm and J. A. Ibers, *Inorg. Chem.*, 2007, **46**, 6992–6996.
63 M. F. Mansuetto, S. Jobic, H. P. Ng and J. A. Ibers, *Acta Crystallogr., Sect. C: Cryst. Struct. Commun.*, 1993, **49**, 1584–1585.
64 W. Nieuwenkamp and J. M. Bijvoet, *Z. Kristallogr. Kristallgeom. Kristallphys. Kristallchem.*, 1932, **81**, 469–474.
65 J.-E. Kwak, D. L. Gray, H. Yun and J. A. Ibers, *Acta Cryst. Sect. E: Struct. Rep. Online*, 2006, **62**, i86-i87.
66 J. Flahaut and M. Picon, *Bull. Soc. Chim. Fr.*, 1958, **6**, 772–780.
67 G. V. Ellert, G. M. Kuz'micheva, A. A. Eliseev, V. K. Slovyanskikh and S. P. Morozov, *Russ. J. Inorg. Chem. (Transl. of Zh. Neorg. Khim.)*, 1974, **19**, 1548–1551.
68 S. Furuseth, L. Brattås and A. Kjekshus, *Acta Chem. Scand., Ser. A*, 1975, **29a**, 623–631.
69 E. Ringe and J. A. Ibers, *Acta Crystallogr., Sect. C: Cryst. Struct. Commun.*, 2008, **64**, i76–i78.
70 L. S. Andrukhiv, L. A. Lysenko, Y. P. Yarmolyuk and E. I. Gladyshevskii, *Dopov. Akad. Nauk Ukr. RSR Ser. A*, 1975, 645–648.
71 S. Bobev, D. J. Mixson, E. D. Bauer and J. L. Sarrao, *Acta Crystallogr., Sect. E: Struct. Rep. Online*, 2006, **62**, i66–i68.
72 Z. Bukowski, R. Troc, J. Stepien-Damm, C. Sulkowski and V. H. Tran, *J. Alloys Compd.*, 2005, **403**, 65–70.
73 D. Kaczorowski, R. Kruk, J. P. Sanchez, B. Malaman and F. Wastin, *Phys. Rev. B: Condens. Matter Mater. Phys.*, 1998, **58**, 9227–9237.
74 J. Yao and J. A. Ibers, *Z. Anorg. Allg. Chem.*, 2008, **634**, 1645–1647.
75 D. M. Wells, G. H. Chan, D. E. Ellis and J. A. Ibers, *J. Solid State Chem.*, 2010, **183**, 285–290.
76 D. L. Gray and J. A. Ibers, *J. Alloys Compd.*, 2007, **440**, 74–77.
77 L. Fournès, M. Vlasse and M. Saux, *Mater. Res. Bull.*, 1977, **12**, 1–6.
78 C. Platte and H. Sabrowsky, *Naturwissenschaften*, 1973, **60**, 474–475.
79 D. L. Gray, G. J. Long, F. Grandjean, R. P. Hermann and J. A. Ibers, *Inorg. Chem.*, 2008, **47**, 94–100.
80 M. G. Kanatzidis and A. C. Sutorik, *Prog. Inorg. Chem.*, 1995, **43**, 151–265.
81 V. M. Fedorov, K. A. Chuntonov, A. N. Kuznetsov, G. A. Bol'shakova and S. P. Yatsenko, *Izv. Akad. Nauk SSSR Neorg. Mater.*, 1985, **21**, 1960–1961.
82 W. G. Moffat, *The Handbook of Binary Phase Diagrams*, Genium Publishing Corporation, Schenectady, New York, 1984.
83 K. A. Chuntonov, A. N. Kuznetsov, V. M. Fedorov and S. P. Yatsenko, *Izv. Akad. Nauk SSSR Neorg. Mater.*, 1982, **18**, 1108–1112.
84 A. C. Sutorik, J. Albritton-Thomas, T. Hogan, C. R. Kannewurf and M. G. Kanatzidis, *Chem. Mater.*, 1996, **8**, 751–761.
85 B. C. Chan, Z. Hulvey, K. D. Abney and P. K. Dorhout, *Inorg. Chem.*, 2004, **43**, 2453–2455.
86 O. Tougait, A. Daoudi, M. Potel and H. Noël, *Mater. Res. Bull.*, 1997, **32**, 1239–1245.
87 J. C. W. Folmer and F. Jellinek, *J. Less-Common Met.*, 1980, **76**, 153–162.

